Journal of Flow Visualization & Image Processing 29(2):43–86 (2022)

A REVIEW ON UNSTEADY FLUID-FLEXIBLE STRUCTURE INTERACTION

Kamal Raj Sharma & Sushanta Dutta*

Aerodynamics Laboratory, Department of Mechanical and Industrial Engineering, Indian Institute of Technology Roorkee, Roorkee, Uttarakhand, India-247667

*Address all correspondence to: Sushanta Dutta, Aerodynamics Laboratory, Department of Mechanical and Industrial Engineering, Indian Institute of Technology Roorkee, Roorkee, Uttarakhand-247667, India; Tel.: +91-1332-285410; Fax: +911332-285665, E-mail: sushanta@me.iitr.ac.in

Original Manuscript Submitted: 8/3/2021; Final Draft Received: 10/19/2021

The present work reviews the flow interactions of structures with flexible configurations in practical applications. The flow dynamics involved in flexible structures under unsteady aerodynamics and changes in the wake morphology of the attached body are covered in this study. Particle image velocimetry data recorded by the authors in their research are summarized. The similarities between the wake structures of rigid and flexible structures attached to bluff bodies are also explored in this article. The results obtained in this study are useful for researchers who wish to understand flow control over streamlined and bluff bodies using flexible structures. In addition, the flow dynamics involved in the flight of natural swimmers and fliers can be understood from this review.

KEY WORDS: *unsteady aerodynamics, fluid–structure interaction, flexible splitter plate, particle image velocimetry (PIV), flexible flapping wing, flapping modes*

1. INTRODUCTION

Unsteady fluid and structure interactions have many practical applications; they include revealing the flow phenomenon involved in the propulsion of natural swimmers and fliers, exploiting the potential and possibilities in energy harvesting, heat transfer augmentations, and the stability of aerodynamic structures. The mechanical system involved in natural fliers and swimmers ensures high efficiency. Simulating such physical problems experimentally and computationally is difficult. The highly flexible structure poses a strongly coupled problem in which the characterization of the flow and structure dynamics is important in order to study the effect of flow dynamics on the structure and the structural forces on the fluid. Such phenomena are common in nature: blood flow and flexible arterial walls, beating of heart muscles, heart wall dynamics, blood flow, fluttering of aircraft wings, helicopters, and turbine blades. These fluid-flexible structures can inspire more innovative designs of artificial systems since they interact with the flow moving around an object.

Recently, the effect of elastic structures on the aerodynamic characteristics of bluff bodies and the reconfiguration of flexible structures under aerodynamic forces have captured the attention of aerodynamicists. A few more applications of interest are flow control of bridge piers, heat transfer augmentation using pin fins with at-

tached flexible splitter plates, design and development of micro-energy harvesters, and flexible flapping-wing micro-aerial vehicles (MAVs). The present study explores the behavior of flexible structures in two aerodynamic applications (1) bluff-body aerodynamics and (2) flapping-wing dynamics. Both flow applications pose unsteady flow conditions for flexible structures. The effects of the fluid–structure interactions are described in this paper. In addition, a comparison between rigid and flexible structures has been drawn.

The wake region created behind the bluff body generates unsteady forces on the bluff body from an early Reynolds number (Re ~ 50), which may cause structural failure due to vibration and fatigue. The vortex shedding phenomenon persists over a wide range of Reynolds numbers, which causes severe structural vibrations due to a significant increase in the fluctuating forces acting on the bodies. Thus, reducing and mitigating this unsteady phenomenon using different flow control methods is vital for various engineering applications. Many researchers have made sincere efforts to suppress vortex shedding behind bluff bodies using active and passive control techniques. Among the active techniques, inline and transverse oscillations of the bluff body (Chauhan et al., 2016; Zhang and Zhu, 2017; Warui and Fujisawa, 1996), suction and blowing on cylinder faces (Rastan et al., 2019), and plasma and synthetic jet actuation (Sosa et al., 2011; Jukes and Choi, 2009; DeMauro et al., 2013; Thomas et al., 2008) are the most extensively used. The most well-known passive flow control techniques are three-dimensional (3D) forces using different shape modifications (Bearman and Owen, 1998; Owen et al., 2000; Park et al., 2006) and the use of control rods (Chauhan et al., 2019) and splitter plates (Chauhan et al., 2018). Splitter plates are considered useful in many passive flow control methods due to their simple design and fabrication. A splitter plate divides the wake of a bluff body into two parts, thus restricting the interactions between staggered and shed vortices. These interactions form a vortex street that leads to the dominating pressure drag in bluff bodies.

Hence, restricting the vortex interaction reduces the bluff-body drag. Moreover, studies have shown that the time-mean drag varies with the rigid splitter plate's length (Mat Ali et al., 2011; Chauhan et al., 2019). Splitter plates of certain lengths can also induce wake transitions due to the shedding of secondary vortices. Various theoretical and experimental studies have brought attention to flow-induced deformations of flexible structures in shear flow caused by bluff bodies. Periodic vortex shedding nearly at constant Strouhal (St) frequency induces such distortions in elastic bodies. Unsteady fluid and structure interactions have many practical applications, including revealing the flow phenomenon involved in the propulsion of natural swimmers and fliers. A few studies have drawn attention to the vortical patterns involved in the wake of flexible splitter-attached bluff bodies. The dynamics of the foil influenced by the fluid have also been addressed in a few studies. The present article reviews the literature related to fluid–structure interactions of the bluff-body wake and unsteady aerodynamics of flexible flapping wings. In addition, the aerodynamic change due to flexible structures is covered in this paper for various geometries.

1.1 Applications of Fluid–Structure Interactions

The application of attached splitter plates have been explored in a few recent studies, including the following:

- Flow control of bridge piers mitigating the local scour at the base of the piers and reducing vibrations (Yu and Yu, 2010)
- Heat transfer augmentation using pin fins with rigid/flexible splitter plates (shown in Fig. 1)
- Use of the integral system of a bluff body and attached flexible foil as a micro-energy harvesting device (Song et al., 2017; An et al., 2018; Liang et al., 2018; Noel et al., 2018)
- To reveal the flow physics involved in the locomotion of natural swimmers and fliers (Shinde and Arakeri, 2014).

2. FLOW CONTROL OVER BLUFF BODIES USING A SPLITTER PLATE

2.1 Particle Image Velocimetry

Particle image velocimetry (PIV) is a measurement technique used to capture all of the flow field velocity information in a fraction of time. It is a non-intrusive, indirect, and whole-field velocity measurement technique that depends on various subsystems to achieve its goal. It is an optical flow measurement technique in which a laser or light-emitting diode source is used to illuminate the tracer particles in the flow field. The particles are illuminated in a plane twice within a short interval of time. The light scattered from the tracer particles has to be recorded on a single frame or sequential frames. Evaluation of the PIV data gives the displacement of the images of the particles between the two light pulses. Complex post-processing is required to handle the large volume of data obtained through PIV measurements. Figure 2 shows a schematic illustration of the

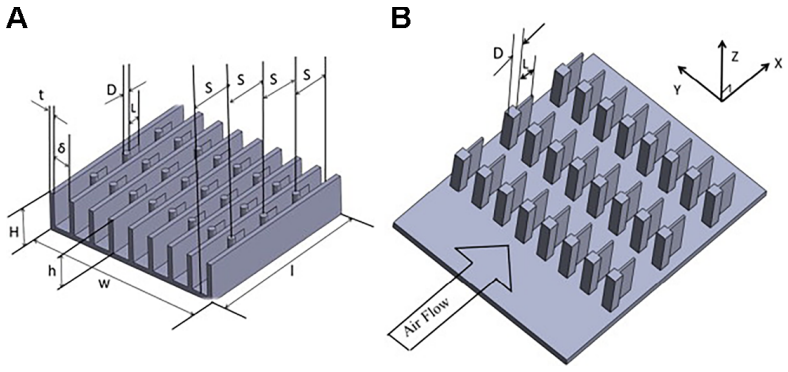

FIG. 1: Application of spitter plate in heat transfer augmentation in pin-fin heat [(a)(reprinted from Razavi et al. with permission from Elsevier, copyright 2015) (b)(reprinted from Sajedi et al. with permission from Elsevier, copyright 2016)]

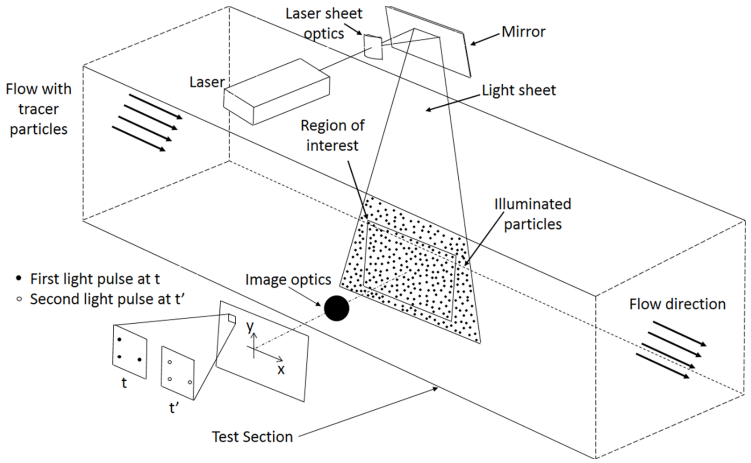

FIG. 2: Schematic illustration of the experimental arrangement of planar PIV

experimental setup of PIV measurements in a water/wind tunnel. The tracer particles are added in the flow, illuminated by the laser sheet twice (the delay in the time between the pulses depends on the velocity of the flow and the calibration factor). It is assumed that the tracer particles follow the streamlines of the flow between the two laser exposures. The scattered light from the tracer particles is captured by a high-quality lens either on a single frame using a camera or on two separate frames using a cross-correlation–based camera.

Next, the optical PIV images are digitized using a scanner and then stored in the memory of a computer for further processing. For processing, the digital PIV data are divided into small subregions called interrogation regions. The local displacement vector is obtained for the PIV images of the first and second exposures for each interrogation region using statistical methods such as auto or cross correlation. It is also assumed that the tracer particles move homogenously within the interrogation region between the two illuminations. The displacement vector then gives the local velocity vector concerning the time duration between the illuminations and the calibration factor. The projections of the local velocity are obtained in the plane of measurements as streamwise and vertical velocities. The process is repeated for all of the interrogation regions in order to obtain the entire velocity field.

Based on the type of illumination and the velocity components achieved, the PIV setup is divided into planar and volumetric PIVs. The PIV setup is characterized by a two-component (2C) or three-component (3C) PIV. The planar PIV is an example of a two-dimensional (2D) and 2C (2D2C) PIV, whereas a stereo PIV is a 2D and 3C (2D3C) PIV and a tomographic or volumetric PIV is a 3D and 3C (3D3C) PIV. Many experimental studies have used PIV to diagnose the effect of splitter plate interference on the flow over bluff bodies. The use of transparent rigid and splitter plates has enabled researchers to measure the flow field on either side of a bluff body. Various flexible splitter plate studies are listed in Table 1.

TABLE 1: Various PIV studies involving flow control using flexible splitter plates

Bluff body	Ref.	Re	AR	*TI* (%)	Methodology	Measurement
Circular	Shukla et al. (2009)	800–10,000	13	—	2D2C PIV	Normalized amplitude and frequency of the plate (A^*)
Circular	Shukla et al. (2013)	1800–10,000	8	—	2D2C PIV	Normalized amplitude and frequency of the plate (A^*)
Circular	Hu and Wang (2013)	420	2.6	0.8	2D2C PIV	Velocity field, vorticity field, and plate dynamics
Circular	Hu et al. (2014)	420	2.1	0.8	2D2C PIV	Velocity field, vorticity field, and plate dynamics
Circular	De Nayer et al. (2014)	30,470	8.18	0.02	2D2C PIV	Flow field
Circular	Teksin and Yayla (2016)	2500	8.3	—	2D2C PIV	Flow field and turbulent stresses
Circular	Teksin and Yayla (2017)	5000	8.3	—	2D2C PIV	Flow field and turbulent stresses
Circular	Yayla and Teksin (2018)	2500–7500	8.3	—	2D2C PIV	Flow field and turbulent shear stress
Square	Binyet et al. (2018)	1500–20,000	7	—	2D2C PIV	Velocity vectors
Circular	Shen et al. (2019)	1500–2500	60	0.5	2D2C PIV	Flow visualization
Circular	Zhou et al. (2019)	924–2268	20.8	0.8	2D2C PIV	Phase-averaged flow field
Circular	Yayla et al. (2019)	2500–7500	8.3	—	2D2C PIV	Flow field and turbulent shear stress
Square	Sharma and Dutta (2020a)	600–2000	20	0.1	2D2C PIV	Flow field and plate dynamics
Square	Sharma and Dutta (2020b)	600–2000	20	0.1	2D2C PIV	Flow field
Square	Binyet et al. (2020)	9200–14,300	7	—	2D2C PIV	Flow field
Circular	Satheesh et al. (2020)	11,300	20	—	2D2C PIV	Plate tip kinematics

TABLE 1: (*continued*)

Bluff body	Ref.	Re	AR	*TI* (%)	Methodology	Measurement
Square	Sharma and Dutta (2021)	600–2000	20	0.1	2D2C PIV	Flow field and plate dynamics
Circular	Duan and Wang (2021)	$(3.83–9.57) \times 10^4$	17	0.3	2D2C PIV	Velocity field measurements

2.2 Rigid Splitter Plate and Bluff-Body Wake

Splitter plates have been widely used as a passive flow control technique for bluff bodies due to their simplicity and effectiveness over other passive methods. Roshko (1954) first introduced passive flow control over bluff bodies using a splitter plate. The author experimentally studied the effect of a rigid splitter plate with a length five times the diameter of a circular cylinder on the lee side of which it was attached. Vortex shedding inhibition was observed over the splitter plate length with a 55% increase in the base pressure and a 40% reduction in the mean drag. Roshko (1954) also studied the effect of a detached-type rigid splitter of one diameter length and varied the distance between the cylinder base and leading edge of the plate. Significant suppression of vortex shedding was observed for the configuration when the distance between the base of the cylinder and the leading edge was 3.85D. The reason behind this trend was a delay in the vortex formation process beyond the trailing edge of the plate. Beyond the critical length, the original mechanism of vortex shedding was restored. Many significant contributions have also been made in the past few decades. Apelt and West (1975) studied the effect of the rigid splitter plate length on the base pressure and vortex shedding characteristics of a circular cylinder in the high subcritical Reynolds number regime experimentally shown in Fig. 3. For L/D = 5, inhibition of the vortex shedding was observed over the

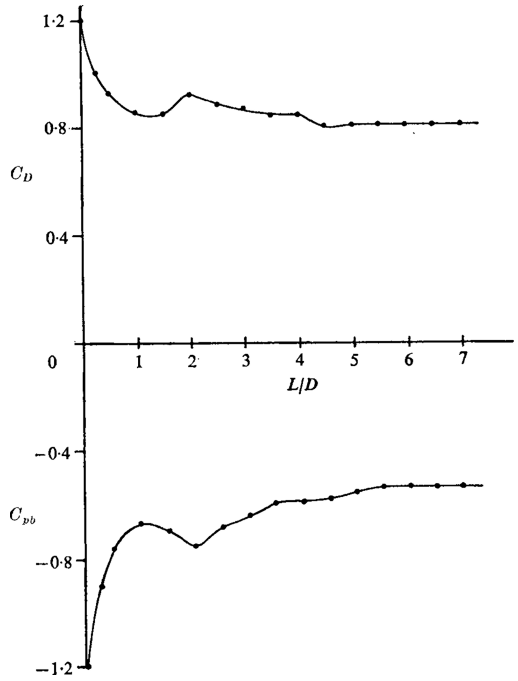

FIG. 3: Variations between the mean drag coefficient (pressure drag) and base pressure and the length ratio of a splitter plate attached to a circular cylinder (reprinted from Apelt and West with permission from Cambridge University Press, copyright 2006)

length of the plate; however, beyond $L/D = 5$, no modification could be achieved except for a further increase in the vortex formation length. Interestingly, for plate length $L/D = 2$, the drag increased to the limit while the Strouhal number was restored to the value of that of the cylinder alone. Apelt and West (1975) attributed this increase in drag to the increase in the wake width; further increase in the splitter plate length caused a small reduction in the drag along with the Strouhal number.

Cete and Unal (1992) numerically investigated an attached rigid splitter plate and its influence on the unsteady wake and derived forces on a circular cylinder. The authors found a monotonic reduction in the bluff-body drag coefficient as the wake splitter length increased from 0 to 2D. The results matched the experimental findings in the literature for lengths up to 0.5D but not for longer splitter plates.

Chauhan et al. (2018) experimentally studied the uniform flow over a square prism with and without an integral rigid splitter. The authors showed the wake flow sensitivity over the splitter plate ratios (L/D) ranged from 0.5 to 6, covering short, medium, and long splitter plates. Various wake regimes were shown for varying lengths of the splitters. The shear layers were stretched before their roll-up for short splitters (L/D = 0.5D–2D), leading to a drop in the vortex shedding frequency. For medium-sized splitters (L/D > 2–4), the primary vortices interacted with the trailing edge of the splitter and shed secondary vortices. The strength of the secondary vortex increased with the length of the wake splitter. For long wake splitters (L/D = 5–6), an increase in the wake formation length was again reported, and the vortex shedding frequency was further suppressed. Chauhan et al. (2018) also showed the consequences of L/D variations on the square cylinder frequency response and drag coefficient, as illustrated in Figs. 4 and 5. Various wake regimes can be observed in Fig. 6, showing the effect of the rigid splitter plate's length on the time-averaged z-component vorticity field.

Noel et al. (2018) introduced the concept of micro-power generators using a rigid splitter plate. The study exploited the galloping response of a prism with different non-circular cross sections (square, trapezoidal, and triangular). The study demonstrated that the useful range of galloping instability could be extended by attaching a rigid splitter plate to the prism rear face. The plate provided a secondary flow reattachment point, which improved the oscillation amplitude, and consequently the generator power output.

Sahu et al. (2019) numerically studied the flow past an elastically mounted cylinder attached to a rigid splitter plate. The study also compared the flow over stationary and elastically mounted cylinders attached to rigid splitter plates. Rigid splitter plates with lengths of L = 1.5D, 2.5D, and 3.5D inhibited vortex shedding at Re = 88, 111, and 145, respectively. The rigid splitter plate reduced the flow fluctuations in the vortex shedding regime when compared to a bare cylinder. The amplitude of the time response of the force coefficients was also reduced using a rigid plate. The rigid splitter plate also reduced the mean drag coefficient considerably, which was caused by the response to the reduction in Reynolds stresses. The increase in the recirculation zone played a small role in the drag reduction. Large fluctuations in the lift coefficient were observed at length L/D = 2.5 and Reynolds numbers greater than 130. In the elastically supported cylinder with a rigid splitter plate, three regimes of reduced velocity were noticed: vortex-

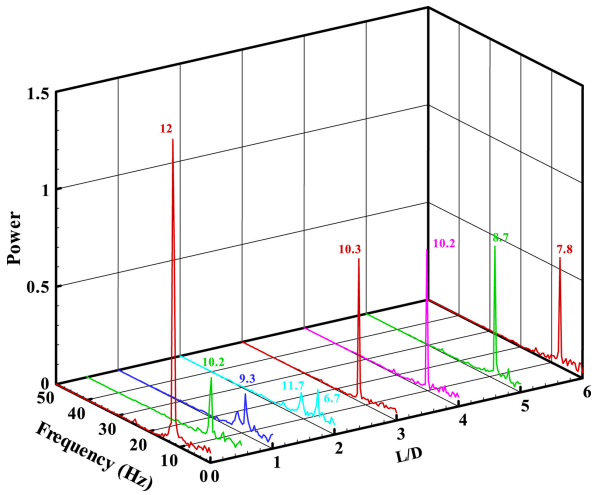

FIG. 4: Power spectra of the streamwise velocity in a square cylinder wake for different length ratios of a rigid splitter at Re = 485 (reprinted from Chauhan et al. with permission from Elsevier, copyright 2018)

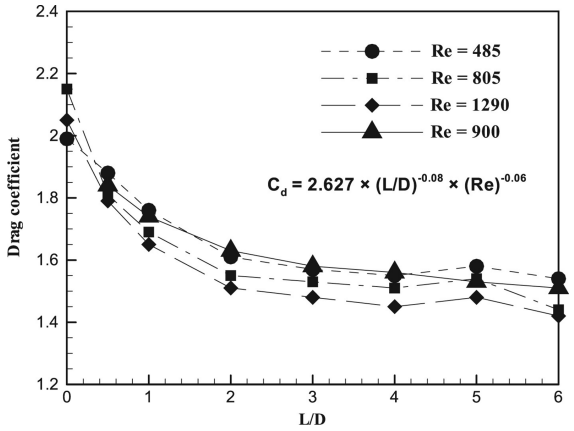

FIG. 5: Mean drag coefficient versus the length ratio of the splitter plate, where the interpolated values are evaluated at Re = 900 (reprinted from Chauhan et al. with permission from Elsevier, copyright 2018)

induced vibration (VIV), steady flow, and galloping. The range of VIVs increased with the length of the splitter. The response in terms of the amplitude of the cylinder–plate system was lower than that of the bare cylinder. A steady flow regime appeared at L/D = 3.5, where vortex shedding disappeared for a reduced velocity range of 11–13.37. A galloping response was observed for highly reduced velocities for all lengths of the plate. The system vibration frequency was lower than its natural frequency and remained constant, increasing the reduced velocity.

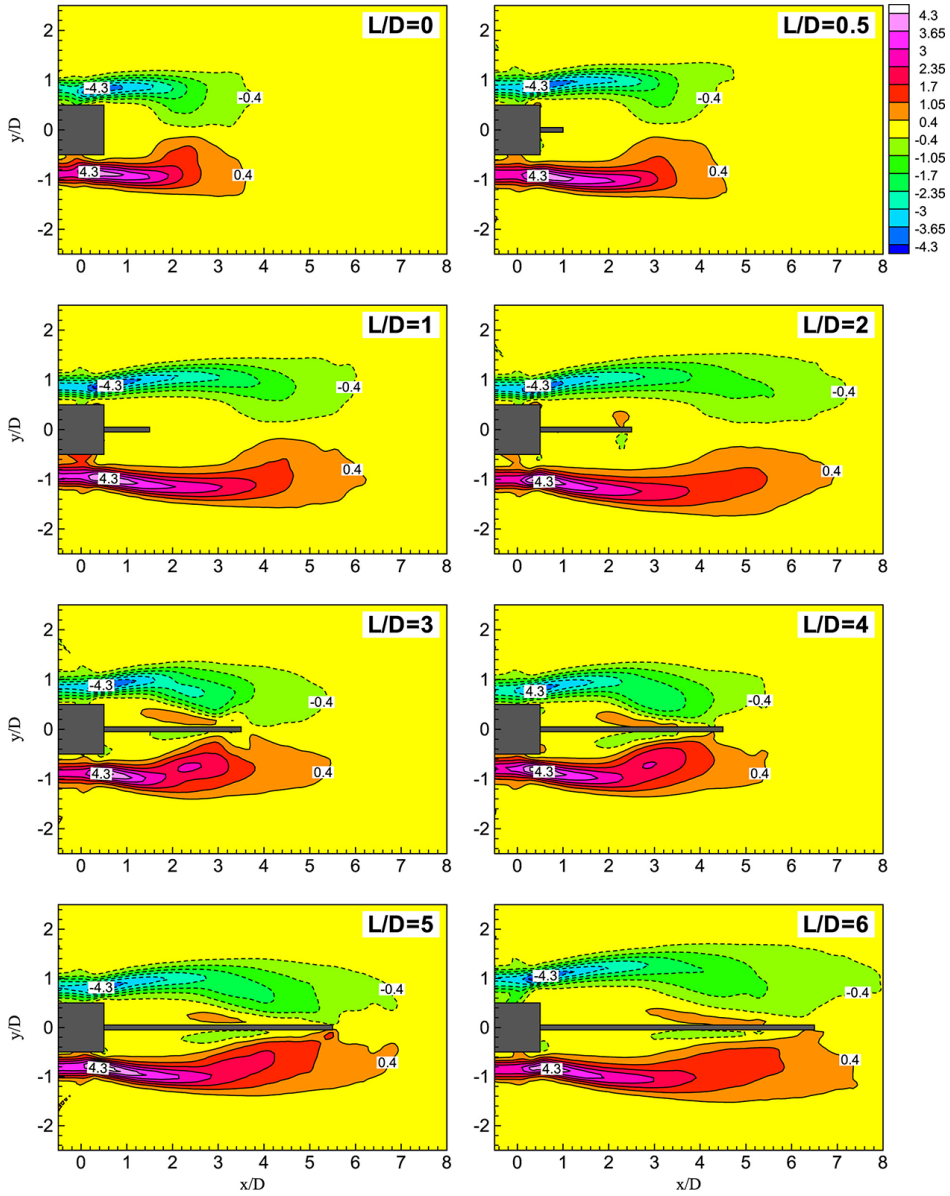

FIG. 6: Time-averaged *z*-vorticity field showing various wake regimes observed for flow over a square cylinder attached to rigid splitter plate of various lengths (reprinted from Chauhan et al. with permission from Elsevier, copyright 2018)

2.3 Flexible Splitter Plate and Bluff-Body Wake

Along with the research studies on rigid splitter plates, several authors were also interested in investigating the interactions between the free shear layers of bluff bodies. The

elastic behavior of a flexible foil is dependent on various non-dimensional parameters, such as the effective stiffness (Π), density ratio (ρ*), and Euler–Bernoulli frequency (the structural natural frequency of *i*th mode, f_{ni}). The mass density ratio ρ* is given by the following equation, where ρ is the density of the flexible foil and ρ_f is the density of the fluid:

$$\rho^* = \frac{\rho}{\rho_f} \tag{1}$$

The effective stiffness (Π) of the flexible foil is given by the followin equation, where *E* is the Young's modulus of the flexible foil:

$$\Pi = \frac{E\left(t/B\right)^3}{12\rho_f U^2} \tag{2}$$

The Euler–Bernoulli frequency (f_{ni}) concerning the *i*th flapping mode of the flexible foil is given by the following equation, which depends on the flexural stiffness (*EI*), geometry (*L* and *t*), and added mass of the surrounding fluid (Jin et al., 2018):

$$f_{ni} = \propto_i \sqrt{\frac{EI}{L^4\left\{\left[\rho_m bt/\left[\rho_f C_m\left(\pi\right)b^2/4\right]\right]\right\}}} \tag{3}$$

Shukla et al. (2009) performed an experimental study in which a rigid splitter was given a free-to-rotate degree of freedom at the hinged base of the circular cylinder. This arrangement allowed some interactions between the two shear layers of the cylinder. The study analyzed the influence of the hinged plate on the flow kinematics and plate dynamics in the range of Re ≈ 800–10,000 by varying the *L*/*D* ratio and mass ratio (ρ*) of the plate. The authors concluded that the flapping amplitude of the plate first increased sharply with the Reynolds number and then changed marginally with a further

increase in the Reynolds numbers. However, when the ρ* value decreased, no effect was found on the plate tip amplitude beyond the value of 0.03. A change in the hinged plate dynamic response was also observed for length ratio L/D = 3–4 at high Reynolds numbers.

Wu and Shu (2011) discussed the effects of the vibration frequency, amplitude, and length of a rigid flapping plate (hinged at the base of the cylinder) on the flow over a cylinder with a circular cross section at low Reynolds number Re = 100. The study was inspired by tadpole locomotion, where the fixed circular cylinder resembled the head and the flapping plate resembled the thin tail of the organism. Numerical simulations revealed that for small plate amplitudes and low flapping rates, the instantaneous drag and lift signatures were irregular, and a weak secondary vortex was shed at the tip of the flapping plate. At larger amplitudes and frequencies, a butterfly shape was observed in the C_D-C_L phase diagrams. During high rates and large-amplitude flapping, the secondary vortex's strength increased. Hence, the primary vortex was affected, and significant changes in the flow structures were observed. For low flapping frequencies, the constructive interaction between the primary and secondary vortices increased the drag, whereas for high flapping rates the destructive mode of the interaction reduced the drag on the cylinder; however, higher flapping rates once again adversely affected the drag characteristics of the cylinder wake.

In two numerical studies, Xiao et al. (2011, 2012) analyzed the impact of a detached foil [National Advisory Committee for Aeronautics (NACA) airfoil NACA 0012] on the flow characteristics of a semi-circular cylinder. The foil was given sinusoidal undulations. In these studies, the authors concluded that the in-between distance of the base of the cylinder and leading edge of the foil had a substantial effect on the flow across the bluff body. The thrust coefficient of the aerofoil increased with the presence of the cylinder when compared to an isolated foil subjected to a freestream. The unity, non-dimensional gap, and unity non-dimensional characteristic length of the bluff body gave the best outcome as concluded in the study, owing to the reverse Karman vortex street. The instantaneous vorticity fields for different gap ratios and two Strouhal frequencies are shown in Figs. 7 and 8.

Since it was observed that undulation bodies affect the wake patterns of bluff bodies, several researchers introduced uniformly elastic splitter plates in the wake of a cylinder and examined their effects using the scenario of a two-way coupled fluid–structure interaction. Bagheri et al. (2012), one of the earliest authors of such studies, numerically studied the effect of an elastic filament attached to a circular bluff body. For an eigenfrequency higher than the Strouhal frequency, the symmetry of the bare cylinder flow was restored with the attached filament since the elastic response of the filament to the strain rate was slow. However, when the Strouhal frequency was dominant, the filament instantly responded to the strain rate, thus spontaneously affecting the flow symmetries and properties. The asymmetric flapping of the elastic plate generated lift without increasing the drag of the cylinder. The study showed that the eigen frequency and Strouhal frequency controlled the dynamic behavior of the flexible filament. The effects of the mass ratio and bending stiffness of the plate were also reported in the study.

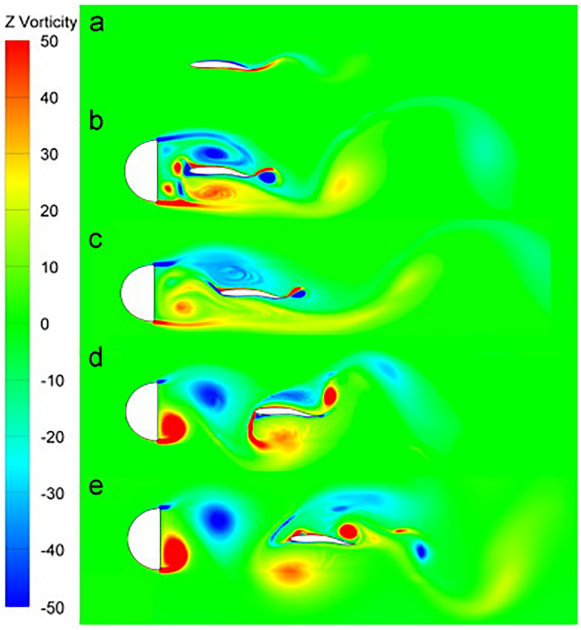

FIG. 7: Instantaneous vorticity contours at $t/T = 0$: (a) $L/D = \infty$; (b) $L/D = 0.5$; (c) $L/D = 1$; (d) $L/D = 1.5$; (e) $L/D = 2$ for St = 0.12 (reprinted from Xiao et al. with permission from Elsevier, copyright 2011)

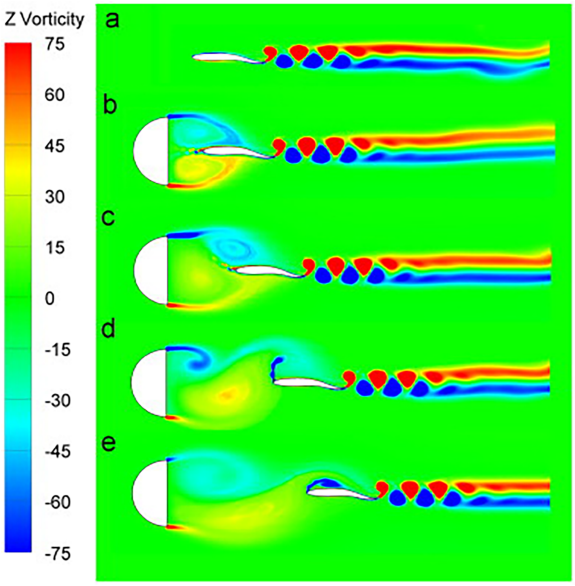

FIG. 8: Instantaneous vorticity contours at $t/T = 0$: (a) $L/D = \infty$; (b) $L/D = 0.5$; (c) $L/D = 1$; (d) $L/D = 1.5$; (e) $L/D = 2$ for St = 0.18 (reprinted from Xiao et al. with permission from Elsevier, copyright 2011)

For the Reynolds number based on the length of the elastic plate, $\mathrm{Re} = L_s U/\upsilon \geq 10^3$, the imposed freestream was strong enough to produce the effect of the mass ratio of the elastic plate. It was seen that for a low mass ratio the flapping of the plate was steady, for an intermediate mass ratio the flapping was periodic, and for a high mass ratio the flapping was chaotic. The bending rigidity stabilized the wake at low values, but higher values destabilized the wake due to upstream influence through modification of the pressure from shed vortices by the trailing edge of the plate.

In their experimental study, Hu and Wang (2013) also observed the flow transition of a flow over a heaving cylinder attached to a flexible tail at Re = 400. The vortex structures were captured using PIV. In the study, various modes were observed in the wake of a cylinder with an attached flexible tail of fixed effective stiffness based on the cylinder diameter ($\Pi = 24$). The density of the material used was such that it matched that of insect wings. Three different flexible tail lengths of varying chordwise effective stiffness ($0.19 \leq \Pi_c \leq 3.0$) were considered in the study, and their effect on the wake structure of the plunging cylinder was reported. For $L/D = 2$ (the tail's length), 2*S* Karman vortex shedding persisted in the wake. 2*P* mode shedding was observed in the wake at $L/B = 3$ and 2*S*-reverse Karman vortex shedding was observed at $L/D = 4$. The wake changed from drag producing to thrust producing at $L/D = 2$ and 4, respectively.

In their experimental study, Shukla et al. (2013) defined the non-dimensional bending stiffness, $K^* = EI/(0.5\rho U^2 L^3)$ (where *EI* is the bending stiffness and *E* and *I* denote the Young's modulus and moment of inertia, respectively), and reported the resuts of the dynamic response of a flexible plate at Reynolds numbers from 1800 to 10000. The amplitude of the flapping splitter plate was observed to vary linearly with the streamwise distance along the wake centerline, as shown in Fig. 9. The amplitude response of the flexible splitter plate to the increase in the Reynolds number showed two periodic oscillation modes (modes I and II) with a large variation in flapping amplitude between the two modes. The amplitude response of the flexible splitter plate was saturated at higher values of the Reynolds numbers in the mode II oscillations. When the effective stiffness of the flexible splitter plate was increased, the amplitude response was shifted to higher Reynolds numbers. The amplitude versus effective stiffness plot converged on a single

FIG. 9: Superimposed images of flexible splitter plate motion at $L/D = 5$ and Re = 8000 (reprinted from Shukla et al. with permission from Elsevier, copyright 2013)

curve of the respective plate length ratio (L/D), as shown in Fig. 10. The short and long flexible splitter plates had similar dynamic behavior; however, plate lengths $L/D = 2$ and 3 gave an aperiodic dynamic response. The unexpected behavior of the plate at $L/D = 2$ and 3 was due to its closeness to the $2D$ formation length of the plain cylinder. Similarly, other studies also characterized the flexibility of the flexible body using stiffness (see, for example, Bagheri et al., 2012; Heathcote et al., 2008; Hu and Wang, 2013; Kang et al., 2011; Sharma and Dutta, 2019).

In a numerical study, Lee and You (2013) found that the Strouhal frequency of the vortex shedding, lift and drag coefficients, and tip displacement changed non-monotonically with the material stiffness of the flexible plate at $L/D = 1$ or 2, and the same parameters were monotonic functions of the material stiffness of the flexible plate at $L/D = 3$. The dynamic response of the plate was observed to depend on the vortex shedding frequency and the flexible plate natural vibration frequency. The deflection shape of the flexible plate depended on the length of the plate, whereas the deflection magnitude was found to be dependent on the material stiffness and natural frequency. The more extended splitter plate effectively modulated the vortex shedding frequency of the cylinder compared to the short or medium splitter plates. The lower stiffness of the plate unfavorably affected the mean drag and lift coefficients of the bluff body.

The numerical studies carried out by Wu et al. (2014a,b) also supported an increase in drag due to the high flexibility of the foil. These studies performed flow control over a circular cylinder using a flexible filament attached to a circular cylinder base. Wu et al. (2014a) used two configurations to keep the cylinder fixed and elastically mounted. The flexibility and length of the flexible filament were varied for the unsteady laminar flow regime (Re = 150) over the cylinder. For a fixed cylinder, the longer lengths of the flexible filament and low flexibility reduced the mean drag force and fluctuations in the lift force better than an isolated cylinder and a cylinder with an attached rigid plate. The

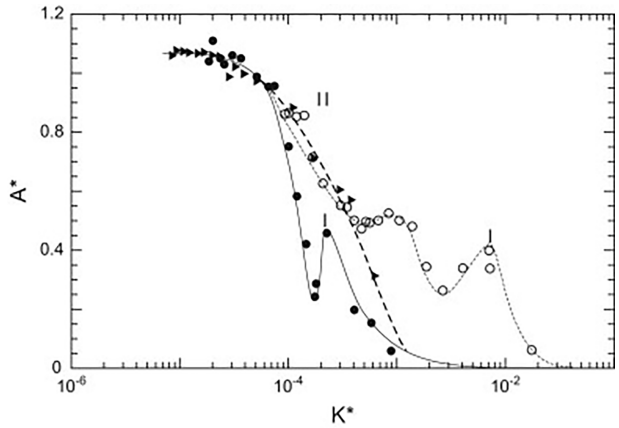

FIG. 10: Variations between the normalized tip amplitude (A^*) and the relative bending stiffness (K^*) for different values of the L/D ratio: $L/D = 3$ (open circles); $L/D = 5$ (closed circles); $L/D = 7$ (triangles) (reprinted from Shukla et al. with permission from Elsevier, copyright 2013)

flapping of the filament potentially increased the pressure behind the cylinder, which reduced the drag.

Moreover, the deflection of the flexible filament pushed the vortices downstream, thus reducing the vortex shedding frequency and lift fluctuations of the cylinder. It was shown that the VIV response of the cylinder was suppressed effectively using long filaments of medium flexibility. The Wu and Shu (2011) study revealed that the suppression was due to the uniformity in the pressure of the upper and lower regions of the cylinder. The destructive interaction of the primary and secondary vortices also helped suppress the VIV response of the cylinder.

Wu et al. (2014b) studied the effect of an undulatory plate on the flow field around a fixed circular cylinder. The Reynolds number was kept fixed at 100. The effect of the frequency and amplitude of the undulation along with the length of the plate was reported in the study. For the length ($l = d$) of the undulatory plate, the flow behavior was governed by the frequency and amplitude of the plate. The mean drag in all of the cases was reported to be less than that of the rigid plate. The mean drag coefficient decreased monotonically at all of the amplitudes considered in the study. For some combinations of frequency and amplitude of the plate, a thrust force was also observed in the wake of the cylinder. The maximum drag reduction increased with the plate length as the strength of the secondary vortex increased in the longer plate.

In a similar study, Wu et al. (2014c) observed the influence of VIVs on a plate hinged to a free-to-move cylinder at a low Reynolds number (Re = 150). The parameters such as the mass ratio ($m^* = 2$), damping ratio ($\zeta = 0$), and plate length ($L = 0.5D$) were kept constant, whereas the effects related to the reduced velocity of the flow and the reduced velocity of the plate were studied. Numerical simulations showed that the plate moderated the variations in the cylinder load characteristics for low and medium reduced velocities. The cylinder without the plate performed better at the high reduced velocity, although the double row vortex street was changed to a single vortex street by the hinged plate. For selected studies of the reduced flow velocity and the ratio of cylinder–plate inertia (I^*), the VIV response of the cylinder was suppressed for a high reduced velocity of the hinged plate along with a large reduction in the drag coefficient and fluctuations in the lift coefficient of the cylinder. The mechanism behind the VIV suppression by the hinged plate was that the secondary vortex shed by the trailing edge destructively interacted with the primary vortex shed by the cylinder.

De Nayer et al. (2014) numerically and experimentally validated a fluid–structure interaction study in a turbulent flow. In the experiments, PIV was used to obtain the phase-averaged flow field of a circular cylinder attached to a flexible plate on the base side at Re = 30,470. The structural deformations were obtained using a laser triangulation sensor. The experimental results were compared to a large eddy simulation with identical geometry and Reynolds numbers. Similar dynamics of the flexible plate were observed in both approaches under consideration. The flexible plate was observed to be flapping in the first swiveling mode, as seen in the PIV results presented in Fig. 11. Figure 11 shows the instantaneous streamwise flow velocity over the circular cylinder attached to a flexible plate at various time instants within a vortex shedding cycle. The

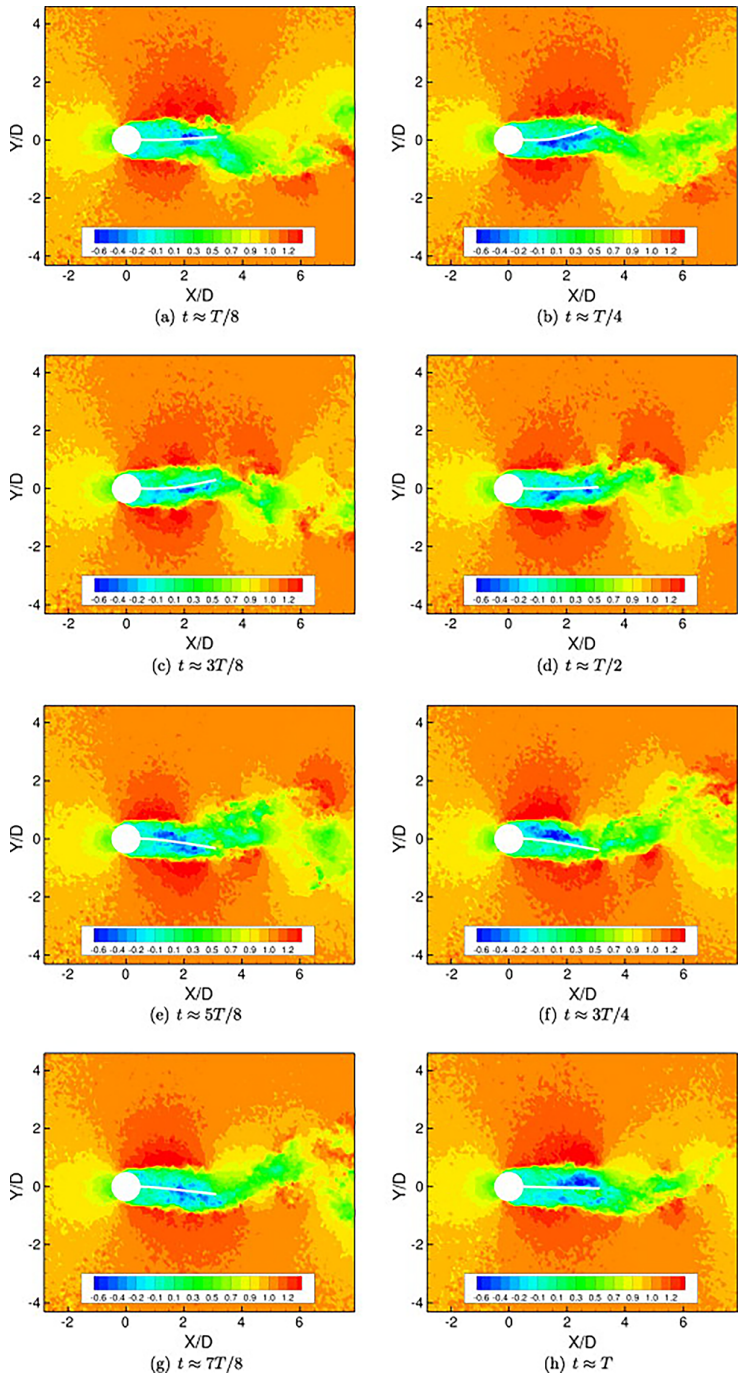

FIG. 11: Instantaneous streamwise velocity of the flow over a circular cylinder attached to a flexible rubber plate at different instants of time over a flapping beat cycle (reprinted from De Nayer et al. with permission from Elsevier, copyright 2014)

Strouhal frequency of the plate was observed to be equal to 0.11. De Nayer and Breuer (2014), in their large eddy simulation of the flow over a circular cylinder integrated with a flexible rubber plate and a rear mass, observed the second mode large deformations of the plate for the subcritical flow regime. The numerical results were compared to previously published experimental results, and good agreement was observed for the frequency, amplitude, and flapping mode of the flexible plate. The effect of the material stiffness of the flexible plate was also introduced in the study. Since rubber material is stiffer under dynamic conditions, the material stiffness obtained from the dynamic test showed good agreement in the three computational structural dynamic schemes.

Kundu et al. (2017) numerically studied the steady and pulsatile flow past an elastic splitter plate attached to a circular cylinder. The study obtained a Strouhal number of the plate flapping and Strouhal number based on its natural frequency. The plate length controlled the flapping mode for the flexible splitter plate. The elastic plate exhibited low-amplitude self-sustained oscillations for steady inflow, and a flow transition was observed as the length of the flexible splitter plate was varied. For a plate of length L/D = 1, the plate flapped at the second natural frequency, and the flapping mode changed to the first natural frequency at L/D = 3.5. The elastic plate experienced strong vortex force by the detaching shear layers for pulsatile flow past the circular cylinder. The maximum amplitude of the plate oscillation was observed when the pulsating frequency of the flow was twice the natural frequency, which is termed the lock-in condition. The beat phenomenon was observed due to the superimposition of the forced flow and the natural frequencies. The total drag was larger than in the steady flow when the forcing frequency was in or over the lock-in frequency for a given amplitude. The increase in the amplitude also increased the skin friction drag and total drag of the cylinder at the lock-in frequency.

Sharma and Dutta (2017) focused on the experimental investigation of Strouhal number modification using a passive flow control technique over a square cylinder placed in the test section of a subsonic low-speed wind tunnel. Rigid and flexible splitter plates attached downstream from the cylinder were used as the passive flow control technique for flow over the cylinder at Re = 400. The lengths of the splitter plates were varied from 0.5D to 8D in order to manipulate the wake behind the cylinder. The hot-wire anemometer measurement technique [constant temperature anemometry (CTA)] was used to characterize the flow in the wake of the cylinder at four downstream locations and various points across the wake. A single wire probe was used to measure the time-averaged and root-mean-square velocities, vortex shedding frequencies, and near and far wake spectra. From the results of the study, the authors inferred that the splitter plate fixed downstream from the square cylinder modified the wake structure and suppressed the vortex shedding phenomenon due to the efficient passive control technique. Reduction in the shedding frequency was achieved in both the rigid and flexible splitter plate experiments. The flexible splitter plate suppressed the vortex shedding phenomenon more effectively than the rigid plate at all splitter plate lengths. The maximum suppression of the Strouhal number by the rigid plate was found to be approximately 65%,

whereas for the flexible splitter plate it was nearly 75% of the Strouhal number of the bare cylinder without a splitter plate at Re = 400.

Liang et al. (2018) performed wind tunnel experiments on the flow over an elastically mounted cylinder attached to a flexible splitter plate with varying effective stiffnesses ($\Pi = 2.33 \times 10^{-4}$ to 2.11, with respect to the length of the plate). The vortex-induced vibrational response of the cylinder was reported to be suppressed by the flexible splitter plate in the range studied ($0.5 \leq L \leq 2.5$). The flexible splitter plate's length greater than 110% of the cylinder diameter caused the galloping kind of instability. The study concluded that the wake transition might result it vortex-induced galloping to the structure, predominantly when a flexible body is attached to the wake side of a square cylinder.

Binyet et al. (2018) performed water tunnel experiments on a rigid square cylinder attached to a flexible polymeric plate. The subcritical Reynolds numbers chosen for the study varied between 15,000 and 20,000. The thickness of the plate was varied to see its effect on both the plate deflection and the flow pattern using PIV. The study showed that at high flexural rigidity, the plate underwent single-mode deflection; however, as the flexural rigidity was decreased, traveling wave deflection and distinct modes of flapping were observed in the plate. The complex deflections of the plate led to higher strain energy states, which confirmed the energy harvesting possibility of the arrangement. Figure 12 shows individual modes of plate deflection as well as the accompanying velocity vectors. It can be noticed from Fig. 12 that the impingement of flow at different locations of the plates is related to the distinct modes of deflection of the plate.

Yayla and Teksin (2018) performed PIV studies on the flow over a circular cylinder attached to a flexible plate in a water channel. Lower subcritical Reynolds numbers were chosen for the study (Re = 2500, 5000, and 7000). Qualitative analysis of the wake structure of a circular cylinder attached to a passive control element was performed in the study. The vortex shedding frequency was also obtained from the PIV data using single-point spectral analysis. The study showed that with a flexible plate, the vortex shedding of the bluff body was altered, and the undulations of the plate mitigated the flow fluctuations. In a similar study, Yayla et al. (2019) presented the turbulent stress and turbulent kinetic energy values of a circular cylinder wake in the presence of an integrated, flexible plate of fixed length, in which the Reynolds numbers were kept equal as in their previous endeavor. A decrease in the peak values of the turbulent stress and turbulent kinetic energy was reported in the study using a flexible splitter plate.

Zhou et al. (2019) experimentally studied the effect of a flexible splitter plate attached upstream of a circular cylinder in the intermediate Reynolds number regime. The effective stiffness of the flexible plate was kept at 1.22, and that of the rigid plate was kept at 1200. The study revealed that the upstream rigid plate did not alter the vortex shedding characteristics of the bluff body, and the flexible splitter plate also behaved as a rigid plate up to a certain Reynolds number. The flexible plate started bending and flapping at a higher Reynolds number (Re = 2268). The flapping plate shed vortices from its trailing edge, which merged with the Karman vortices of the bluff body downstream. The interaction of the trailing edge and Karman vortices affected the Strouhal frequency of the wake, and the effect increased with the bending of the flexible splitter plate. The

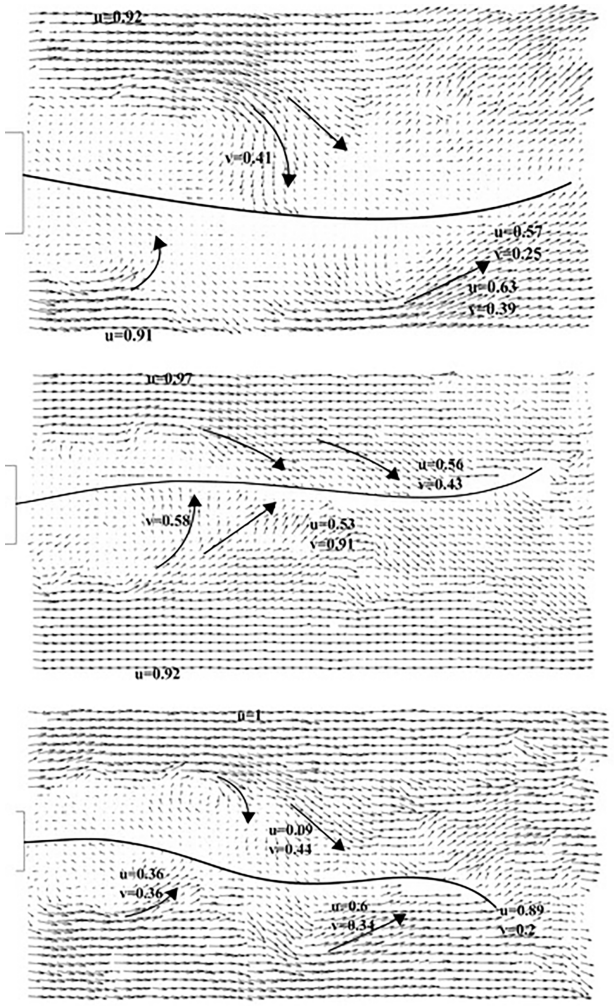

FIG. 12: Different modes of complex bending of an attached flexible plate (top to bottom: from the first mode to the third mode) due to impingement of the flow at different locations of the plate (reprinted from Binyet et al. with permission from Microsystem Technologies, copyright 2018)

process of merging the upstream and downstream Karman vortices did not alter the original shedding mode.

Another experimental study by Shen et al. (2019) revealed the effect of the Reynolds number and length of a flexible film attached to a circular bluff body. The material stiffness of the film was kept unchanged at $E = 1.99 \times 10^6$ N/m^2. The results showed that the pressure spectrum amplitude for the attached flexible film exceeded that for a bare cylinder. In addition, the flapping film of length $L/D = 3$ brought a complicated frequency component behind the wake flow. The study also confirmed the upstream movement of the flow transition for the bare cylinder as the Reynolds number increased

from 1500 to 2500. The film flapped asymmetrically in the wake and resulted in asymmetric pressure fluctuations.

In their experimental investigation of flow control over a square cylinder, Sharma and Dutta (2020a) found individual wake regimes for different lengths of a flexible splitter at an intermediate Reynolds number (Re = 600). The flow visualization images for this configuration are shown in Fig. 13. The time-averaged coefficient of drag was varied non-monotonically due to the distinct wake regimes. Substantial primary and secondary vortex interference caused a wake transition between $L/B = 3$ and $L/B = 4$. Low-amplitude undulations of the flexible plate stabilized the square cylinder wake and reduced the time-averaged coefficient of drag.

Sharma and Dutta (2020b) imaged the flow field behind a stationary square cylinder with attached rigid and flexible splitter plates using PIV, CTA, and flow visualization techniques. A wide range of lengths of the splitter plate (L/B = 0–8) was considered, and their respective wake interference was reported. The investigation was carried out at an intermediate flow regime at three Reynolds numbers, namely 600, 1000, and 2000 (based on blocking width B of the cylinder). The study showed that the wake frequency and mean drag coefficient varied non-monotonically for the splitter plate length. The length of the splitter plate was reported to be a critical parameter, which apart from flow control also brought a significant wake transition. At $L/B > 3$ to $L/B = 4$, strong secondary vortices were shed from the trailing edge, as shown in Fig. 14. The secondary vortex shedding led to a sudden shrinkage in the recirculation bubble, increasing the unsteady flow periodicity. The onset of high-amplitude flapping occurred in the flexible splitter plate ($L/B = 3$) at Re = 2000. The vortex shedding frequency became higher than the first mode natural frequency of the flexible splitter plate for $L/B = 3$ and remained in this regime for $L/B > 3$. The flapping amplitude increased up to $L/B = 5$ and then receded again, as shown in Fig. 15. The high-amplitude flapping of the flexible splitter plate adversely affected the time-averaged drag coefficient of the bluff body.

Binyet et al. (2020) simulated anguilliform locomotion swimming in an experiment on the flow over a square cylinder attached to a flexible plate. Strain energy was presented as a parameter to check the efficacy of the flexible plate as an efficient energy harvester. The parametric effect of the square cylinder diameter and the thickness and length of the plate on the wake was investigated using PIV and fluid–structure interaction modeling. The study revealed that long plates gave larger power output but lower conversion efficiencies, and the cylinder diameter and plate thickness parameters should be chosen according to the incoming velocity range.

Satheesh et al. (2020) performed experiments to study the effect of the free surface formation on the flow characteristics of a circular cylinder attached to flexible splitter plates with two different bending rigidity magnitudes. The hydrodynamic forces acting on the integrated system were also presented in the study at subcritical Reynolds numbers. The experiments were performed in a recirculating open surface water channel. The load cell measurements provided the hydrodynamic drag and lift acting on the cylinder with a flexible splitter plate. High-speed camera images were used to track the deflection of the flexible splitter plate. It was reported in the results that rigid and flex-

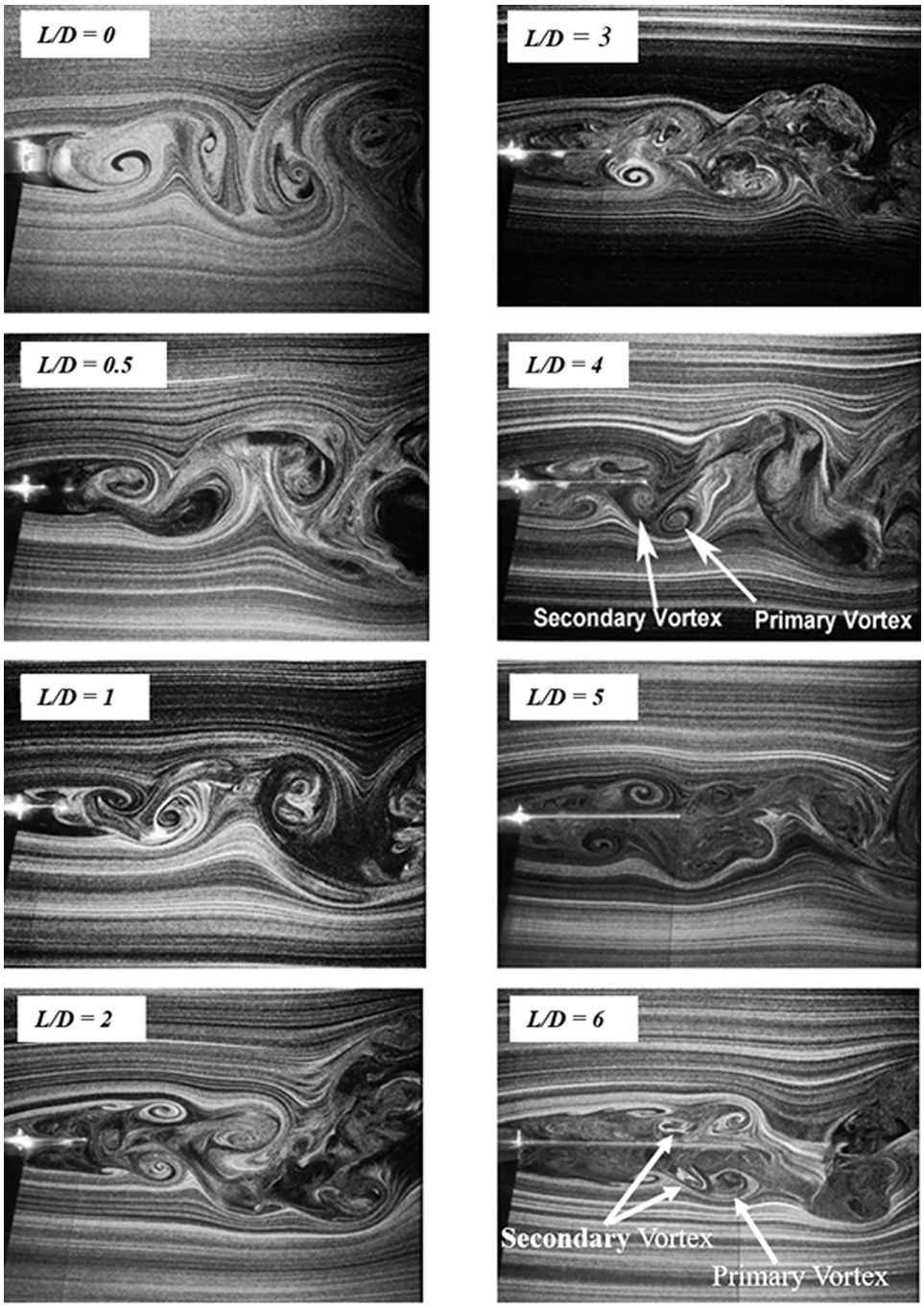

FIG. 13: Particle streaks at Re = 600 and L/D = 0, 0.5, 1, 2, 3, 4, 5, and 6 of a flexible wake splitter attached to a square cylinder (reprinted from Sharma and Dutta with permission from Begell House, copyright 2020)

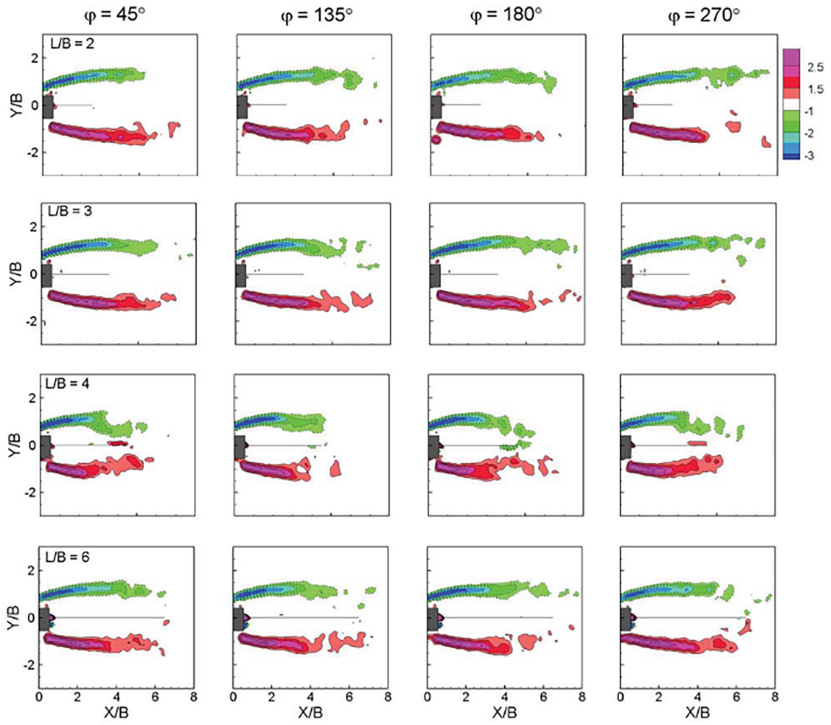

FIG. 14: Phase-averaged non-dimensional spanwise vorticity field for various lengths of a flexible splitter plate at different phases, φ (reprinted from Sharma and Dutta with permission from AIP Publishing, copyright 2020)

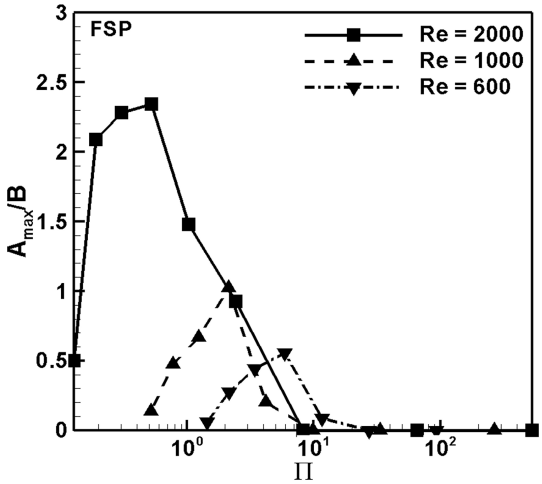

FIG. 15: Maximum non-dimensional tip amplitude versus effective stiffness (Π) for a flapping flexible splitter plate at subcritical Reynolds numbers (reprinted from Sharma and Dutta with permission from AIP Publishing, copyright 2020)

ible splitter plates showed a lower drag coefficient but a higher lift coefficient in the bare cylinder case, where the rigid splitter plate outperformed the flexible splitter plate.

Sharma and Dutta (2021) experimentally investigated the effect of the stiffness of a flexible splitter plate on the flow in a square cylinder in the low subcritical Reynolds number regime. PIV and hot-wire anemometry were used to obtain the spatial and temporal flow parameters. The kinematics of the flexible plate was recorded by high-resolution images captured by the PIV setup. The study showed that the flapping state of the flexible splitter plate depended on the resonance of the vortex shedding frequency and the natural frequency of the flexible plate. In the study, two modes of flapping based on the linear resonance were observed, as shown in Fig. 16, and their respective instantaneous vorticity plots as the effective stiffness (Π) varied. The effects of the length and effective stiffness of the plate on the Strouhal frequency and time-averaged drag coefficient are shown in Fig. 17. It can be noticed in Fig. 17 that the Strouhal frequency and time-averaged drag coefficient vary non-monotonically with the length of the flexible splitter plate and the effective stiffness significantly affects the wake transition as well as the drag coefficient. The time-averaged drag coefficient was seen to be a function of the linear resonance of the Strouhal and natural frequencies of the plate. The asymmetric bending mode was not reported in the study.

Sun et al. (2021) performed low Reynolds number flow simulations of a flexible splitter plate attached to a square cylinder. The bending rigidity of the plate was varied over three orders of magnitude, and the non-dimensional length of the flexible plate was varied as 0.5, 1, and 2 at Re = 100. The study showed that for non-dimensional length = 0.5 (l/L, where L is the side of the square cylinder), the flexible plate oscillated at low amplitude in the first mode since the flow frequency dominated the first mode natural frequency of the plate. For l/L = 1, lock-in between the first mode natural frequency of

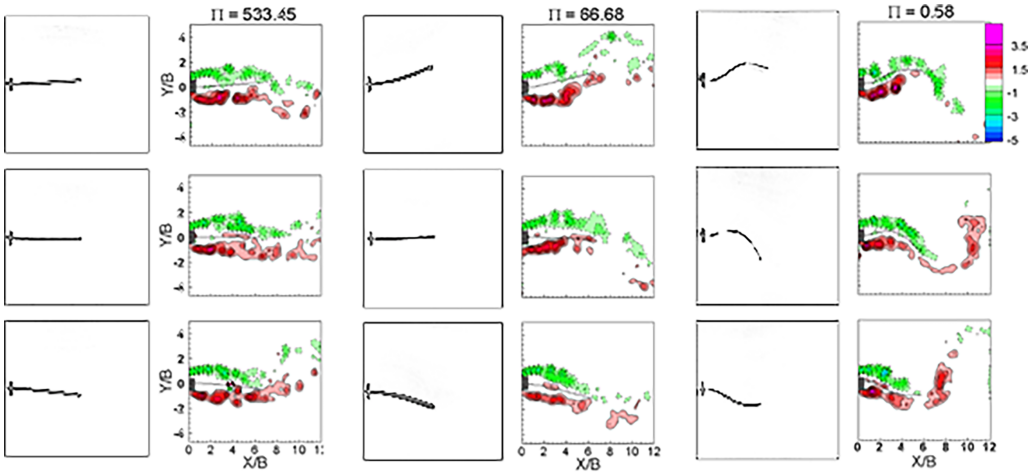

FIG. 16: Different flapping modes of a flexible splitter plate of length L/B = 6, along with their respective spanwise vorticity fields at Re = 2000 (reprinted from Sharma and Dutta with permission from Elsevier, copyright 2021)

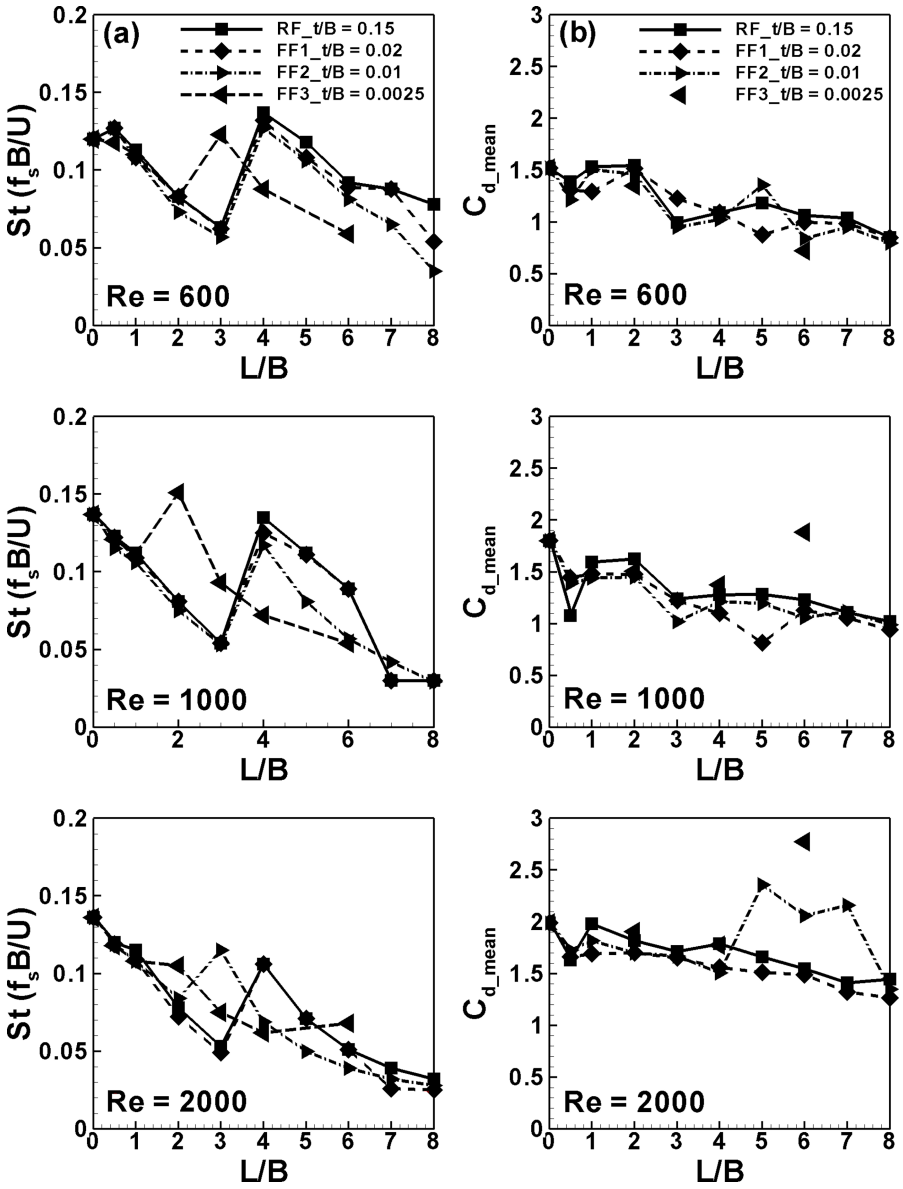

FIG. 17: Modifications of the Strouhal number (a) and mean drag coefficient (b) of a square cylinder flow due to variations in the length and stiffness of a flexible splitter plate at lower subcritical Reynolds numbers (reprinted from Sharma and Dutta with permission from Elsevier, copyright 2021)

the plate and the vortex shedding frequency was observed, and larger oscillations in the first mode were observed in the plate, as seen in Fig. 18. For l/L = 2, the plate oscillated in the first mode at high rigidity, whereas at lower rigidity the plate underwent asymmet-

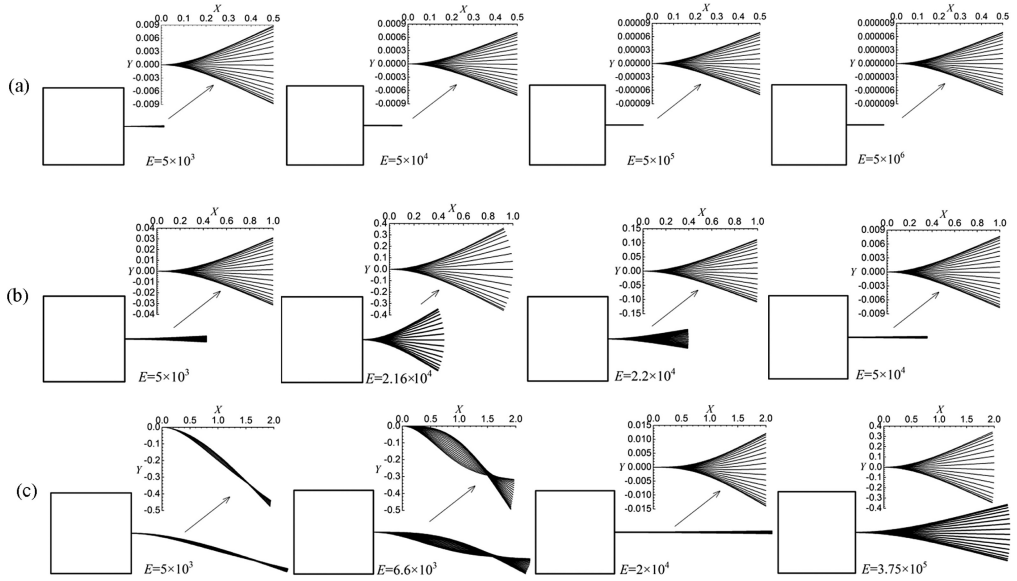

FIG. 18: Flapping dynamics of a flexible splitter plate in the square cylinder flow (a) l/*L* (non-dimensional length of the plate, where *L* is the width of the cylinder) = 1, (b) l/*L* = 1, and (c) l/*L* = 2 (reprinted from Sun et al. with permission from Elsevier, copyright 2021)

ric oscillations in the second mode since the second mode natural frequency dominated the Strouhal frequency, as shown in Fig. 18. The flow structures related to other dynamic regimes of the flexible plate were also presented in the study.

Duan and Wang (2021) experimentally investigated the effects of rigid and flexible splitter plates on the aeoline tone of a circular cylinder. The study covered the higher subcritical flow regime, where the Reynolds number was varied from 3.83×10^4 to 9.57×10^4. The non-dimensional length of the splitter plate was varied from 0.5 to 6. The velocity field was measured using a 2D2C PIV system, whereas the flexible plate deformation was captured using a single camera and a 3D digital image correlation algorithm. The source of the aeoline tone was reported to be the flow fluctuations in the near wake. The study showed that $L/D = 1$ is the optimal length of aeoline noise reduction, where the flexible splitter plate performed better than the rigid splitter plate. Although the flexible splitter plate optimally reduced the aeoline tone, it simultaneously increased the high-frequency noise content.

3. UNSTEADY AERODYNAMICS OF A STREAMLINED BODY

3.1 Flexible Flapping Structure

Streamlined flapping structures show high lift and thrust characteristics on a miniature scale. The fluid–structure phenomenon generates unsteady aerodynamic characteristics, comprised of leading-edge vortices (LEVs), trailing-edge vortices, and wakes. If the

flapping structure is flexible, it undergoes rapid deformation under such unsteady flow conditions because of the high degree of freedom. Due to the practical applications of this phenomenon, many studies have been performed to understand the complexity of the problem. The governing parameters involved in the fluid–structure interaction are the Reynolds number, advance ratio or Strouhal number, density ratio, effective stiffness, and reduced frequency. The Reynolds number is defined in the following equation, where U_∞ and U_{tip} are the freestream and wingtip velocities, respectively; c is the mean chord of the structure; and υ is the fluid kinematic viscosity:

$$\mathrm{Re} = \frac{\left(U_\infty + U_{tip}\right)\mathrm{c}}{\upsilon} \tag{4}$$

The advance ratio is defined in Eq. (5) as the ratio of the freestream velocity to the wingtip velocity, where the wingtip velocity is given as $U_{tip} = 2\phi fR$. Here, ϕ is the flapping amplitude, f is the flapping frequency, and R is the half-wing span:

$$J = \frac{U_\infty}{U_{tip}} \tag{5}$$

The reduced frequency is defined in Eq. (6). It is a measure of the unsteady behavior of the structure and depends on the flapping frequency, aspect ratio (AR), and mean chord:

$$k = \frac{\pi f \mathrm{c}}{U_\infty} \tag{6}$$

The ratio of the density of the structure (ρ_s) and the density of the fluid (ρ_f) is called the density ratio, which is given by the following equation:

$$\rho^* = \frac{\rho_s}{\rho_f} \tag{7}$$

The effective stiffness of the structure is defined in Eq. (8) as the ratio of the bending force to the aerodynamic force. Here, E is the elastic modulus of the structure and h_s is the thickness of the structure:

$$\Pi = \frac{E\left(h_s/c\right)^3}{12\rho_f U_\infty^2} \tag{8}$$

Dickinson et al. (1999) measured the aerodynamic forces acting on a dynamically scaled model of a *Drosophilia* insect. The wing kinematics of the insect were mimicked in the model. The experiment was performed in a vessel containing mineral oil, and the wings were translated for a constant wingtip velocity maintained at Re = 136 (similar to the case of an insect in flight). Constant velocity rotation was also incorporated during the wing reversals in the flapping system along with the translational motion. The force coefficients for the pure translational motion were compared with the translating and rotating wing aerodynamic forces to obtain the rotational force and force coefficient. The rotational force was experienced due to the Magnus effect, as explained by the authors. The rotational force signatures were connected to the force transients observed at the stroke reversals. The advancement and delay in wing rotation with the wing reversal considerably affected the rotational forces. The advanced wing rotation approach was proven to enhance the lift in the model. The active control of the wing rotation between the wings was suggested to be the reason for the efficient flight control of insects. The subtraction of translational and rotational forces from the total force measured gave the aerodynamic force due to wake capture. The study thus explained the possible kinematics and dynamics involved in insect flight.

In relation to insects, the Ellington (1999) investigations showed that the wing area is proportional to $m^{2/3}$, where m is the mass. The wing beat frequency increased with a decrease in size since there is an inverse relation between the frequency and the mass ($m^{-1/4}$). The Reynolds number was based on the mean chord and mean wingtip velocity; therefore, the Reynolds number varied with the value of m. An advance ratio (J) characterized the unsteady aerodynamics of wings with natural fliers. During hovering, the advance ratio (J) was zero, and it increased as the forward flight increased and the body tilted nose down. At high J values, asymmetry was pronounced. The downstroke was powerful, giving both lift and thrust, but the upstroke gave mainly thrust. The top

speeds of the insects were limited because of the advance ratio. Very little thrust was required for the insects, being only 10%–20% of the weight of the insect. Hence, during the design of MAVs, the hovering characteristics should be checked first. In the design of MAVs, up to 100 mm of the wing span, similar to an insect in flight, can be reasonably practical.

Gluck et al. (2001) presented one of the earliest computational fluid dynamics (CFD)/computational structural dynamics (CSD) coupled numerical methods for fluid–structure interaction problems. The coupled algorithm was applied to simple test cases such as the deformation of a flexible vertical plate fixed at the bottom in a flow field at Re = 50. A second L-shaped plate was also investigated. The tip displacements were evaluated for both geometries. Damped oscillations were obtained in both simulations. Finally, a real-life textile tent structure of glass–fiber synthetics with a complex shape was taken into account. This example was investigated under turbulent flow model pressure distribution and displacement distribution conditions over the tent surface in the *z*-direction.

Sane and Dickinson (2002) mimicked insect flight using a dynamically scaled model. The rotational forces were measured for a flapping wing, steadily translating and rotating at the stroke reversals, with constant velocities. The total force transients were compared with the outcomes of 2D quasi-steady modeling. The difference between the model estimates and the measured total force gave the rotational force, and the rotational coefficient thus obtained was compared with 3D mathematical modeling developed using a blade element theory. A discrepancy was reported between the measured rotational force coefficients and the mathematical estimates since the angular velocity was varied. The mathematical model was modified using the measured rotational force coefficients to include the effects of the rotational forces and added mass along with the translational forces. Thus, the model estimates yielded forces due to wake capture, which were then subtracted from the total measured force.

Sun and Tang (2002) conducted a numerical analysis of a model fruit fly wing under conditions of unsteady aerodynamics. The wing motion in the model imitated the wing motion of a fruit fly in hovering flight. The momentum equations were numerically solved, which provided the pressure and flow fields. The vorticity structures and aerodynamic forces were also obtained. The authors found that maximum lift was obtained by three mechanisms: (1) fast acceleration of the wing at a beginning stroke, (2) no stalling during a stroke, and (3) rapid wing pitching at the end of a stroke. The lift was comparatively smaller when half-wing rotation was performed near the end of one stroke and the beginning of another stroke. The time-averaged lift was more than 80% of the quasi-steady value. Likewise, the third possibility of the smallest time-averaged lift was also discussed.

Ho et al. (2003) reviewed the aerodynamics of a flapping-wing flier. The authors also presented a few examples of piezoelectric devices with closed-loop control to change the wing shape. Scaling laws were summarized that related to different parameters of natural fliers. The unsteady flow regime was characterized by limiting the advance ratio (J) for natural and synthetic fliers. The vortex-controlled unsteady aerodynamics was

also explained. The natural and synthetic methods of flow control under separated flow conditions were compared.

Heathcote et al. (2004) simulated the hovering of insects and birds through towing tank experiments of a flexible foil attached to a plunging hydrofoil in a zero freestream. The objective of the experimental study was to investigate the effect of the foil stiffness on the hydrodynamics. The PIV measurement was performed to obtain the flow behavior around the plunging airfoil, and the load measurements gave the extent of the hydrodynamic forces acting on the foil. The relative bending stiffness of the flexible foil was varied as 1:8:512. An alternating vortex street was observed in the wake of the flexible foil. The vortex strength, lateral spacing, and time-averaged induced jet velocity were recorded, which depended on the foil flexibility, plunge frequency, and amplitude. The direct force measurements confirmed that the thrust coefficient for the intermediate stiffness was the greatest at high plunging frequencies, although the foil with the least stiffness generated larger thrust at low frequencies. The propulsive efficiency of the flexible foil was found to be greater than that of the stiffer foil.

Miao and Ho (2006) numerically studied the unsteady aerodynamics of a flapping airfoil due to the flexural amplitude in the chordwise direction. Various combinations of reduced frequencies and Reynolds numbers were chosen. The study covered a range of flexural amplitudes from 0 to 0.7 times that of the chord length at $Re = 10^4$ and reduced frequency, $k = 2$. The pressure coefficient was obtained along the span for different values of the flexural amplitude on both faces of the airfoil. In addition, the effect of variations of the k value on the propulsive efficiency was plotted as a function of the Reynolds number. The drag and thrust regions were shown, suggesting that a minimum k value was required at different Reynolds numbers. Enhancement in the propulsive efficiency was observed at a flexural amplitude 0.3 times that of the chord length. The highest propulsive efficiency was found at Strouhal number $St = 0.255$.

Watman and Furukawa (2008) presented a visualization system to analyze MAV-scaled flapping wings. By synchronizing the wings being tested, multiple devices were triggered at exact phases in the flapping cycle with a high degree of accuracy and repeatability. System-controlled devices such as strobe lights, lasers, and cameras simultaneously captured wing motion and flow visualization data at the point of interest. The system was developed, implemented, and tested under ideal and real-world conditions to evaluate several performance aspects. The effectiveness of the system was also demonstrated in a flow visualization experiment, which was used to capture images of normal airflow around a flapping wing at several wing phases. The performance measurements showed high measurement accuracy, while the flow visualization results demonstrated significant improvements in the quality and accuracy of the images when the system was used to analyze a flapping wing. These results indicate the potential of the measurement approach to considerably improve visualization analysis of MAV-scaled flapping wings.

Heathcote et al. (2008) studied the effect of spanwise flexibility on flapping-wing propulsion in a water tunnel, in which the chord-based Reynolds number was varied between 10,000 and 30,000. The chordwise rigid wings were given heaving motion at one end. The range of Strouhal numbers observed in the experiments was 0.2–0.4, falling in

the range of values seen in natural fliers. Lift and thrust forces were measured by a load cell. The PIV system measured the flow field over three configurations of NACA 0012 rectangular wings: inflexible, flexible, and highly flexible. The AR of the wings was fixed at a value of 6. Loss in thrust was observed for the highly flexible wing, whereas a 50% increase in thrust was reported for the compliant wing.

Cai et al. (2008) performed a numerical simulation to understand the flow characteristics of an aerofoil with a wavy tail. The effects on the drag coefficient, wavelength of the wave disturbance, vortex shedding mechanism, and frequency were examined. A wavy trailing edge with a constant amplitude and wavelength (five times the base height) produced the most significant reduction in the time-averaged drag. The reduction in drag was attributed to an increase in the size of the recirculation region, mitigation of velocity fluctuations, and a relative increase in streamwise vortices. The authors concluded that the presence of a vortex shift could be linked to a reduction in drag.

von Ellenrieder et al. (2008) explained the fluid mechanics of flapping wings based on 2D flapping-wing studies. The selection of the Strouhal number was explored in the design, modeling, and control of flying systems. The study supported the formation of a spanwise flow that affected the LEV because it balanced the generation and shedding of the vortex.

Hu et al. (2009) conducted an experimental study to determine the aerodynamic benefits of using flexible membrane wings in MAVs. One rigid wing and two flexible wings were considered, keeping their planform area equal. Wood and nylon and latex sheets were used as wing membrane materials. A low-speed wind tunnel was used in the experiments. The first set of experiments was performed on soaring flight to measure the lift and thrust coefficients. Experiments were then performed on flapping flight, and the thrust and lift forces were compared to those under soaring conditions. A force–moment sensor measured the aerodynamic forces. The authors concluded that flexible wings had aerodynamic benefits over rigid wings since the lift and thrust of rigid wings fell drastically at a high angle of attack. Furthermore, drag was higher in the rigid wing. The nylon wing membrane performed best in the soaring test, but the latex wing membrane outperformed it in the flapping-wing flight tests.

Akaydın et al. (2010) placed short-length piezoelectric beams in the wake of a circular cylinder at a high Reynolds number. The performance of the piezoelectric beams was evaluated as an energy generator. Similar vortical structures in the flow produced a periodic force on the beam and gave a maximum output voltage when matched to its resonance. The beam had dimensions of 30 mm × 16 mm × 0.2 mm. The first natural frequency of the beam was 48.4 Hz, and the second was 310 Hz. The experiment was performed in a wind tunnel that provided up to 11 m/s air velocity. The Reynolds number ranged from 10,000 to 21,000, with resonant frequency occurring at Re = 14,800. The Strouhal number was constant at 0.2. The vibrations of the beam produced almost 0.148 μW. The maximum power output with a given beam was about 4 μW, which occurred at $y = 0$ and $x/D = 2$.

Mazaheri and Ebrahimi (2010) investigated the aeroelastic effects of flexible wings on the hovering and cruising aerodynamic performance. A flapping-wing system and

an experimental setup were designed and built. The study measured the unsteady aerodynamic and inertial forces, power usage, and angular speed of the flapping-wing motion for different flapping frequencies and various wings in relation to their chordwise flexibility. The aerodynamic performance of the vehicle under both no wind (hovering) and cruise conditions was also investigated. The results showed how elastic deformations caused by the interaction of inertial and aerodynamic forces acting on the flexible structure might specifically affect power consumption. This information was used to find a more suitable structural design. The best-selected design in these tests performed up to 30% better than the others (i.e., less energy consumption for the same lift or thrust generation).

Ashraf et al. (2011) numerically studied the influence of the thickness and camber of an airfoil cross section on airfoil motion. Mere plunging motion and a combination of plunging and pitching movements were tested on the airfoil. Variations in the Reynolds numbers were carried out. NACA 2D symmetric airfoil with thicknesses varying from 6% to 50% was the material chosen for the experiments. Reduced frequency k was kept at a value of 2 in each study. For pure plunging motion, the amplitudes (h) were fixed at 0.25 and 0.5. For simultaneous plunging and pitching, the amplitude was kept at 0.5, and a phase angle of 90° was chosen. The pitch angles were kept at 15° and 30°. At lower Reynolds numbers, thin airfoils performed better than thick airfoils. The thick airfoil gave higher thrust and propulsive efficiency than the thin airfoil in pure plunging and combined flight conditions at higher Reynolds numbers. The camber had little influence on the thrust of the airfoil.

Marais et al. (2012) experimentally studied the effect of pitching rigid and flexible aerofoils at Re = 1035. Time-resolved PIV measurements were performed to diagnose the nature of the flow dynamics. The study focused not only on the thrust effect of the flapping foil but also on the stability of the propulsive wake. In the case of the rigid foil, the transition in the wake took place at two stages. In the first stage, the Benard–von Karman vortex street changed to a reverse Benard–von Karman vortex street; in the second stage, symmetry breaking took place in the wake and the wake became asymmetric. The first wake transition remained unchanged in the flexible foil, but the second wake transition was absent in the flexible foil. The symmetric wake was entirely inhibited by flexible foil flapping.

Hua et al. (2013) numerically studied the propulsion of a flexible flapping plate in a stagnant, incompressible, and viscous fluid. The leading edge of the plate was given a sinusoidal heaving motion. The entire plate moved due to the fluid–structure interaction. Three discrete motions of the plate were recognized: forward, backward, and irregular. These states depended on the heaving amplitude and flexural rigidity of the plate. Two different vortex streets existed in the flapping plate wake: normal and deflected. It was concluded that the appropriate extent of flexibility in the forward motion regime could increase the propulsion performance.

Tronchin et al. (2013) solved the problem of directly measuring low aerodynamic forces in flapping flight through sensors. The authors evaluated the loads on a flapping wing from the integration of the momentum equation. The forces and 3D pressure

distribution were evaluated numerically after measuring the velocity fields around the flapping wing using the PIV technique. A NACA 0012 airfoil was flapped in a water tank. The StarCCM software program was used to perform a numerical analysis of the integration of the momentum equations. The Reynolds number was kept fixed at 1000. The results suggested that sufficient accuracy was obtained in the calculated pressure field. An estimation of the aerodynamic forces from the integrated pressure distribution on the wing surface was accurately achieved.

Lee et al. (2014) numerically studied the dynamics of a flapping flag in a uniform flow stream. The mass ratio of the flag, the surrounding ambient and bending rigidities of the flag, and the Reynolds number were the governing parameters in the system. Three flapping conditions were observed in the flag at a low Reynolds number (Re = 200): stretched-straight state, regular flapping state, and irregular flapping state. The dominant frequency of the flag trailing edge matched with the frequency of the most dominant coherent structures identified using dynamic mode decomposition of the streamwise velocity. Irregular flapping was associated with two distinctive frequencies, and the chaotic flapping mode gave a broadband frequency response.

Goushcha et al. (2014) studied a cantilever piezoelectric beam when immersed in airflow subjected to naturally occurring vortices. The vortices were formed using a loudspeaker analogous to those behind bluff bodies. The results of the pressure distribution and deflection of the beam were presented, as well as the results of the strain and PIV measurements for an individual vortex and multiple vortices over the beam. The results showed that the beam first moved downward and then upward during the individual vortex studies when the vortex cores passed above the beam.

In an experimental study, Deshpande et al. (2014) compared flow field measurements obtained by PIV and flow visualization using smoke on four types of planform of rigid wings and one planform of a flexible wing. The material used for the wing membrane was a Perspex sheet of 3 mm thickness, while the span was 150 mm, and the chord was 80 mm for all wings. The symmetrical stroke amplitude was kept constant at 80°, and the flapping frequency was varied from 0.277 to 2 Hz. The rigid wings generated LEVs of nearly equal strength. The LEVs were stronger for the flexible wing compared to the rigid wing. In the flexible wing, the LEVs were small and near the wing surface. Because of the increased vorticity and closeness of the wing surface, the aerodynamic performance of the flexible wing was better than that of the rigid wing.

Shinde and Arakeri (2014) performed an experimental study of the flow over a pitching airfoil (NACA 0015) attached to a flexible foil at its trailing edge in quiescent flow. The pitching amplitude varied from ± 10° to ± 20° over a range of frequencies. The flexible foil had fixed flexural rigidity. The Reynolds number was defined based on the velocity of the trailing edge of the foil. The airfoil without the flexible foil generated a deflecting jet that caused meandering of the wake, as shown in Fig. 19. The flexible foil, when attached, created a coherent undulating jet and shed vortices in a reverse Benard–Karman vortex street. The flexible foil increased the inter-vortex spacing between the shed vortices, which inhibited dipole formation, which was the main reason behind the meandering of the wake.

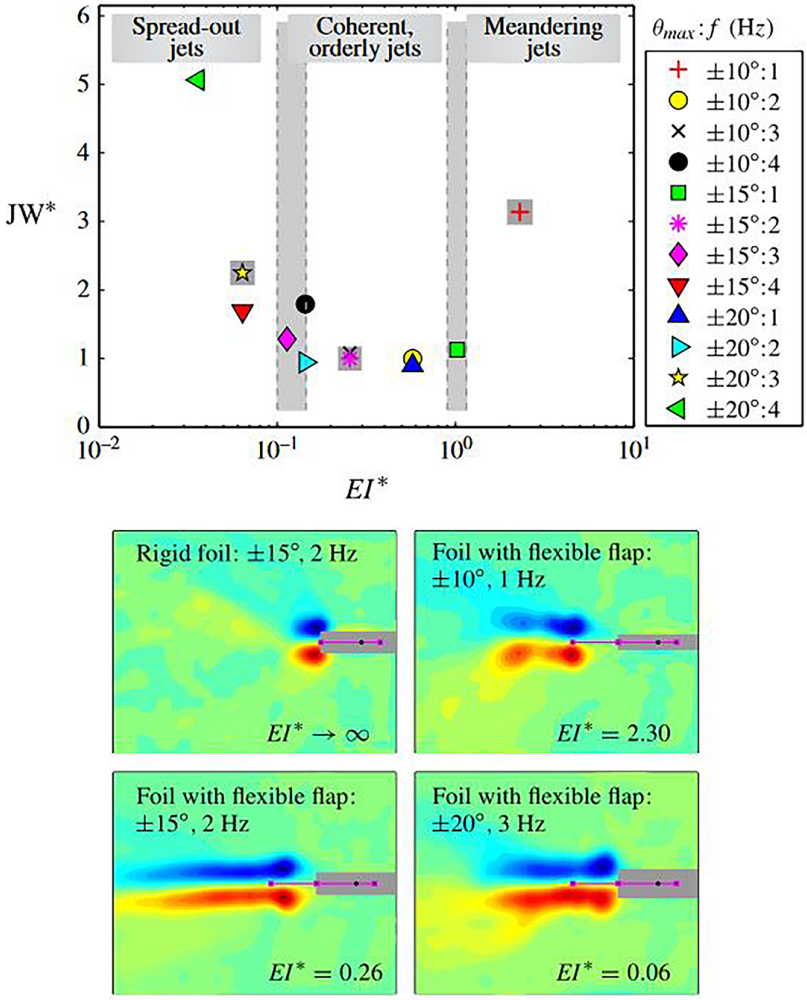

FIG. 19: Normalized jet width (JW) versus the effective stiffness of a flexible flap: the vorticity plots show the representative cases of deflected (upper two contours), coherent (lower-left contour), and spread-out (lower-right contour) jets, highlighted by the gray square in the JW*-*EI** plot (reprinted from Shinde and Arakeri with permission from Cambridge University Press, copyright 2014)

Csaba et al. (2014) studied three rectangular wings with ARs of 1, 2, and 4. A wingtip-based Reynolds number of 5300 was kept fixed for all of the wings. Amplitude Φ was also kept constant at 120°. The experiments were conducted in a glass-walled water tank (1200 × 800 × 1000 mm) at zero freestream velocity. The wings were placed at three times the chord distance from the wall; therefore, wall proximity effects were neglected. PIV was used for flow visualization, and the images were recorded as a function of the azimuthal angle and various spanwise locations. The authors concluded that the

LEV occupies a significant portion of the chord for wings with larger ARs. No significant effect of the tip vortex on the LEV was found.

Ryu et al. (2015) numerically studied the inverted flag problem in a uniform upstream flow using an immersed boundary method. The flapping of the flag and wake structure were observed in terms of the Reynolds number and bending rigidity of the flag. Three dynamic flapping modes were observed in the flag: deflected flapping, symmetric flapping, and straight no-flapping. The transitional mode in between the straight flapping and straight modes was termed the biased mode. Various vortex shedding modes were observed in the wake of the flag (P, $P + S$, and $2P$ modes) since the bending rigidity and flapping frequency were varied. The P mode gave the maximum strain energy and was realized for intermediate bending rigidity and high flapping frequency (nearly $f = 0.2$). The inverted flag with P mode shedding was suggested as an efficient energy harvester system.

Jin et al. (2018) performed PIV and particle tracking velocimetry experiments on three bottom wall–mounted thin plates with different tip geometries: rectangular, semi-elliptical, and aristate. PIV was used to measure the flow field around the thin plates, and particle tracking velocimetry was used to observe the plate dynamics. The study showed that the narrower tip of the thin plates induced less turbulence and drag in the wake of the plate. The turbulence mainly governed the plate dynamics near the plate tip and nonlinear variation of the structural flexure.

Chen et al. (2018) presented and validated an unsteady aerodynamic model for a flexible flapping wing with variable camber. A 2D rigid airfoil model based on the potential flow theory was extended in the present study for a rigid airfoil with variable camber and finally to a 3D flexible wing. The symmetric rigid foil produced zero lift averaged over the beat cycle since the lift produced in the downstroke was equivalent to the negative lift produced in the upstroke. After giving a positive camber of 9% at the mid-upstroke, the negative lift in the upstroke was reduced by 21%. When the elastic deformation of the asymmetric flexible wing was taken into account, the negative lift was reduced by 24% in the upstroke, and the mean lift coefficient was found to be more than that obtained for the cambered rigid foil.

Ryu et al. (2019) performed a 3D simulation over a heaving flexible plate free to move in the streamwise direction. The leading edge of the flexible plate oscillated in the transverse direction. The ratio of the trailing-edge width to the leading-edge width was given the symbol S. Different trapezoidal shapes of the flexible plate were tested along with the rectangular plate as a special case ($S = 1$). The AR of the plate was fixed at 0.4. The cruising speed, power input, and propulsive efficiency were analyzed for different S values of the plate. The maximum cruising speed was obtained at a flapping frequency (f) that was 1.09 times the natural frequency (f_{fluid}) of the plate in the fluid; however, the propulsive efficiency was maximum at $f/f_{\text{fluid}} = 1.5$ and $0.25 \leq \text{St} \leq 0.4$. Maximum propulsive efficiency was found for the plate at $S = 0.5$. The instantaneous vortical structures around the flexible flapping foil are shown in Fig. 20 for two different S ratios, namely, rectangular and trapezoidal.

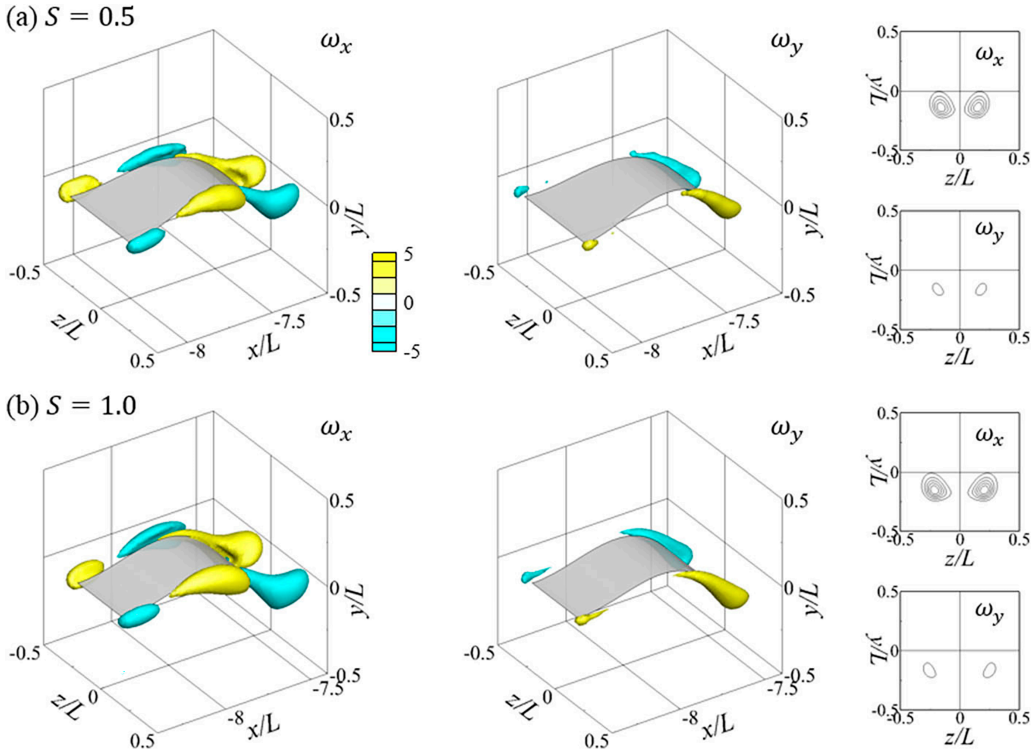

FIG. 20: Instantaneous vortices around the flapping flexible foil as a function of the shape ratio (*S*) (reprinted from Ryu et al. with permission from AIP Publishing, copyright 2019)

Qin et al. (2020) studied the two-way fluid–solid coupled problem for a bio-inspired flexible flapping flap using CFD and CSD. The change in the material properties of the flexible flap changed its aeroelastic behavior. An appropriate selection of flap stiffness generated a large lift and backward airflow leading to a large forward thrust. For the highly flexible flap, increased resistance in the horizontal direction was observed due to large deformations of the flap, which in turn decreased the flight efficiency of the flap. The study concluded that flexibility improved the aerodynamics of the wing; however, too much wing flexibility could result in adverse effects on the flight efficiency and energy consumption.

Deng et al. (2020) designed and fabricated a bio-inspired flapping-wing MAV (FMAV) that mimicked the flight of *Allomyrina dichotoma*. High-speed photography of *A. dichotoma* was performed to observe the deformation of the wings of a natural flier during flight. The designed FMAV could flap at an amplitude of 160° with a maximum flapping frequency of 50 Hz. The FMAV could perform multiple maneuvers such as pitch, roll, and yaw to mimick the attitude of the natural flier. The prototype could generate a maximum lift of 28.6*g* and enough torque to perform maneuvers. A six-axis load sensor was used to measure the aerodynamic forces generated by the prototype attached to a three degrees of freedom platform. Table 2 give a comparison of the key parameters of the natural flier and the designed prototype.

TABLE 2: Comparison of key parameters of *A. dichotoma* and the FMAV (Deng et al., 2020)

Paramter index	Length (mm)	Width (mm)	Wing span (mm)	Chord (mm)	Weight (g)	Frequency (Hz)	Amplitude (°)
A. dichotoma	45	30	160	15	10	50	150
FMAV	45–60	30–40	160–220	15–35	15–25	25–50	120–160

Addo-Akoto et al. (2021) experimentally studied the role of flexibility and wing kinematics of a flapping-wing model. Digital PIV experiments were performed to study the unsteady hydrodynamics of hovering flight of rigid and flexible flapping wings at Re = 10^4 in a quiescent ambient water tank. The force transients were measured using a six-axis load sensor. Rectangular-shaped rigid (acrylic, 2 mm thick) and flexible (polyester, 0.025 mm thick) wings were fabricated. The study concluded that the effect of rotational timing was observed more in the rigid wing than the flexible wing, and the flexible wing load characteristics showed a phase delay in relation to the timing of rotations. The increase in the sweep duration increased the lift in both wings. The flexible wings generated extra lift at the end of the stroke due to stored elastic energy in the form of camber and twist. The negative force transients present in the case of the rigid wings undergoing delayed and advanced rotations were eliminated by the flexible wings, as shown in Fig. 21. The sinusoidal sweeping reduced the negative force transients in the rigid flapping wing. As shown in Fig. 22, trailing-edge vortices were observed closer to the flexible wing surface than to the rigid wing surface. The linear twist of the flexible wing caused the LEVs to be strongly attached to the wing. Hence, the flexible wing delayed the radial limit of the dynamic stall in comparison to the rigid wing.

4. CONCLUSIONS

The present study covered a literature review on passive flow control over bluff bodies using a flexible splitter plate. The effects of rigid and flexible splitter plates on the wake characteristics of bluff bodies and the drag coefficient have been described. In flexible splitter plates, the effective stiffness and Reynolds number affect the dynamics of flow and plate movement. Only a few studies have reported plate dynamics in the context of its natural frequency, which is a function of the effective stiffness. For stiffer flexible plates, the wake behaves similar to the rigid splitter plate. Plate lengths from 2 to 4 times the bluff-body diameter cause wake transitions similar to the rigid splitter plate. The flexible splitter plate has been proven to be a better passive flow control device than the rigid splitter plate since it breaks the fixed point instability and starts flapping. Low-amplitude flapping involves the first mode of flapping, synchronized with the first natural frequency mode of the plate, which stabilizes the bluff-body wake.

In contrast, high-amplitude flapping involves higher flapping modes, which adversely affect the drag coefficient. For fixed bluff bodies, the only drag-producing wake was reported for various flapping ranges of a flexible splitter plate. However, for elastically mounted bluff bodies free to heave in the transverse direction, a thrust-producing

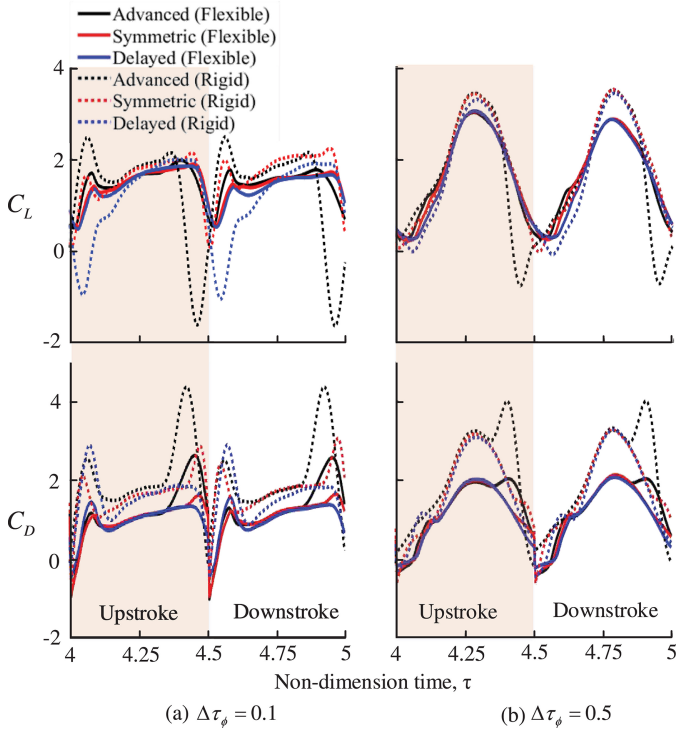

FIG. 21: Comparison of instantaneous forces for the fifth flapping cycle of rigid and flexible flapping wings for two different sweep durations (reprinted from Addo-Akoto et al. with permission from Elsevier, copyright 2021)

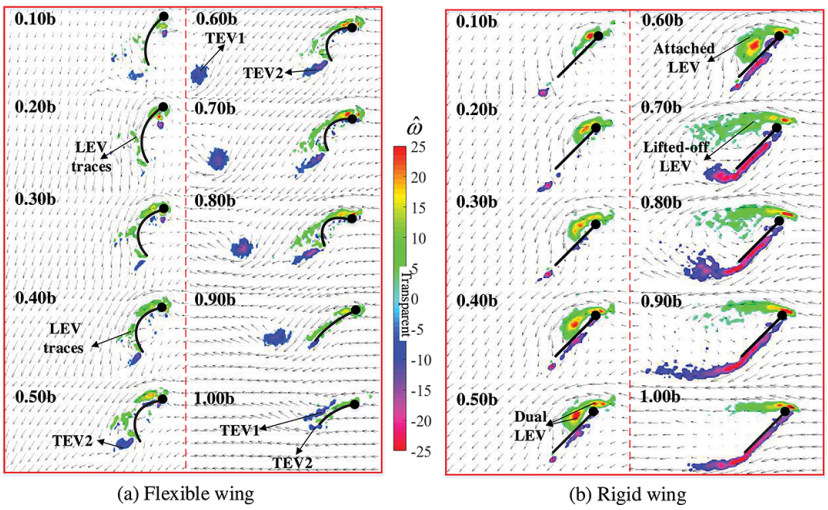

FIG. 22: Spanwise vorticity at a flapping instant for symmetric rotation and constant sweep duration (reprinted from Addo-Akoto et al. with permission from Elsevier, copyright 2021)

wake was also reported beyond some critical length of the flexible splitter plate. When attached to streamlined bodies in the limiting case of high-to-infinite Strouhal numbers, the flexible splitter plate showed a tendency to mitigate flow meandering and produced a coherent jet-producing wake for a specific range of kinematic parameters of the immersed bodies. A few studies used the cylinder–flexible splitter plate system as a micro-energy harvester, proving its potential in diverse applications. Overall, the flexible splitter plate is an important flow control device with many applications in emerging engineering fields.

Various flexible structure interactions with quiescent and flowing fluid media have been reviewed in this article, leading to applications of flow control or energy harvesting possibilities. The gist of all of these studies was similar to the results discussed for flexible splitter plates, namely, that a compliant degree of flexibility gives better results than rigid counterparts and even more so compared to highly flexible structures. A flexible flapping structure attached to a rigid foil inherently provides a thrust-producing wake. Only a few studies have reported a reduction in the wake turbulence, and a few others have reported mitigation of flow meandering and the production of coherent jets for pitching rigid bodies attached to flexible foils. The flexible structures achieved different dynamic modes in the upstream flow depending on the Reynolds number of the assembly and the frequency of the natural mode. The shape of the flexible structure is also a performance factor since it affects the strength and orientation of the vortical structures. Overall, the flexible structure proves to be an efficient flow control device; however, it needs to be carefully designed to avoid adverse effects on aerodynamic performance. Many studies concerning flexible foils were done for limiting cases of Strouhal numbers in the range of the linear unsteady flow regime ($St > 0.1$ and angles of attack $< 15°$). The literature lacks studies on the effect of flexibility in nonlinear and unsteady flow regimes. The drag-to-thrust–producing characteristics have not been well understood in the literature. Moreover, most of the studies considered uniform flow conditions when studying fluid–structure interactions, whereas in practical situations the flow characteristics may change randomly. Hence, studies are required to understand the fluid–structure interactions in flows of varying turbulence intensity and shear flow environments.

REFERENCES

Addo-Akoto, R., Han, J.-S., and Han, J.-H., Roles of Wing Flexibility and Kinematics in Flapping Wing Aerodynamics, *J. Fluids Struct.*, vol. **104**, p. 103317, 2021. DOI: 10.1016/j.jfluidstructs.2021.103317

Akaydın, H.D., Elvin, N., and Andreopoulos, Y., Wake of a Cylinder: A Paradigm for Energy Harvesting with Piezoelectric Materials, *Exp. Fluids*, vol. **49**, no. 1, pp. 291–304, 2010. DOI: 10.1007/s00348-010-0871-7

An, X., Song, B., Tian, W., and Ma, C., Design and CFD Simulations of a Vortex-Induced Piezoelectric Energy Converter (VIPEC) for Underwater Environment, *Energies*, vol. **11**, no. 2, pp. 1–15, 2018. DOI: 10.3390/en11020330

Apelt, C.J. and West, G.S., The Effects of Wake Splitter Plates on Bluff-Body Flow in the Range $10^4 < R < 5 \times 10^4$. Part 2, *J. Fluid Mech.*, vol. **71**, no. 1, pp. 145–160, 1975. DOI: 10.1017/S0022112075002479

Ashraf, M.A., Young, J., and Lai, J.C.S., Reynolds Number, Thickness and Camber Effects on Flapping Airfoil Propulsion, *J. Fluids Struct.*, vol. **27**, no. 2, pp. 145–160, 2011. DOI: 10.1016/j.jfluidstructs.2010.11.010

Bagheri, S., Mazzino, A., and Bottaro, A., Spontaneous Symmetry Breaking of a Hinged Flapping Filament Generates Lift, *Phys. Rev. Lett.*, vol. **109**, no. 15, pp. 1–5, 2012. DOI: 10.1103/PhysRevLett.109.154502

Bearman, P.W. and Owen, J.C., Reduction of Bluff-Body Drag and Suppression of Vortex Shedding by the Introduction of Wavy Separation Lines, *J. Fluids Struct.*, vol. **12**, no. 1, pp. 123–130, 1998. DOI: 10.1006/jfls.1997.0128

Binyet, E., Huang, C.-Y., and Chang, J.-Y., Characterization of a Vortex-Induced Vibrating Thin Plate Energy Harvester with Particle Image Velocimetry, *Microsyst. Technol.*, vol. **24**, no. 11, pp. 4569–4576, 2018. DOI: 10.1007/s00542-018-3935-x

Binyet, E.M., Chang, J.-Y. and Huang, C.-Y., Flexible Plate in the Wake of a Square Cylinder for Piezoelectric Energy Harvesting—Parametric Study Using Fluid–Structure Interaction Modeling, *Energies*, vol. **13**, no. 10, p. 2645, 2020. DOI: 10.3390/en13102645

Cai, J., Chng, L.T., and Tsai, H.M., On Vortical Flows Shedding from a Bluff Body with a Wavy Trailing Edge, *Phys. Fluids*, vol. **20**, no. 6, p. 064102, 2008. DOI: 10.1063/1.2931682

Cete, A.R. and Unal, M.F., Effects of Splitter Plate on Wake Formation from a Circular Cylinder: A Discrete Vortex Simulation, *Comput. Fluid Dyn.*, vol. **1**, pp. 349–57, 1992.

Chauhan, M.K., Dutta, S., and Gandhi, B.K., Wake Flow Modification behind a Square Cylinder Using Control Rods, *J. Wind Eng. Ind. Aerodyn.*, vol. **184**, no. 2019, pp. 342–361, 2019. DOI: 10.1016/j.jweia.2018.12.002

Chauhan, M.K., Dutta, S., Gandhi, B.K., and More, B.S., Experimental Investigation of Flow over a Transversely Oscillating Square Cylinder at Intermediate Reynolds Number, *J. Fluids Eng.*, vol. **138**, no. 5, pp. 1–19, 2016. DOI: 10.1115/1.4031878

Chauhan, M.K., Dutta, S., More, B.S., and Gandhi, B.K., Experimental Investigation of Flow over a Square Cylinder with an Attached Splitter Plate at Intermediate Reynolds Number, *J. Fluids Struct.*, vol. **76**, pp. 319–335, 2018. DOI: 10.1016/j.jfluidstructs.2017.10.012

Chen, S., Li, H., Guo, S., Tong, M., and Ji, B., Unsteady Aerodynamic Model of Flexible Flapping Wing, *Aerosp. Sci. Technol.*, vol. **80**, pp. 354–367, 2018. DOI: 10.1016/j.ast.2018.07.017

Csaba, J.F., Qiu, H., and Shyy, W., Research Paper Effects of Aspect Ratio on Flapping Wing Aerodynamics in Animal Flight, vol. **30**, pp. 776–786, 2014.

DeMauro, E.P., Leong, C.M., and Amitay, M., Interaction of a Synthetic Jet with the Flow over a Low Aspect Ratio Cylinder, *Phys. Fluids*, vol. **25**, no. 6, p. 064104, 2013. DOI: 10.1063/1.4811710

De Nayer, G. and Breuer, M., Numerical FSI Investigation Based on LES: Flow past a Cylinder with a Flexible Splitter Plate Involving Large Deformations (FSI-PfS-2a), *Int. J. Heat Fluid Flow*, vol. **50**, pp. 300–315, 2014. DOI: 10.1016/j.ijheatfluidflow.2014.08.013

De Nayer, G., Kalmbach, A., Breuer, M., Sicklinger, S., and Wüchner, R., Flow past a Cylinder with a Flexible Splitter Plate: A Complementary Experimental–Numerical Investigation and a New FSI Test Case (FSI-PfS-1a), *Comput. Fluids*, vol. **99**, pp. 18–43, 2014. DOI: 10.1016/j.compfluid.2014.04.020

Deng, H., Xiao, S., Huang, B., Yang, L., Xiang, X., and Ding, X., Design Optimization and Experimental Study of a Novel Mechanism for a Hover-Able Bionic Flapping-Wing Micro Air Vehicle, *Bioinspiration Biomimetrics*, vol. **16**, no. 2, p. 026005, 2020.

Deshpande, P., Antony, R., Narayanan, P., Rajashesan, A., Singh, D., and Ramesh, G., Visualization and PIV Measurements of Leading-Edge Vortex Generated by Rigid Flapping Wings of Different Planforms, *AIAA Aviation*, vol. **32**, pp. 2014–2880, 2014.

Dickinson, M.H., Lehmann, F.O., and Sane, S.P., Wing Rotation and the Aerodynamic Basis of Insect Right, *Science*, vol. **284**, no. 5422, pp. 1954–1960, 1999. DOI: 10.1126/science.284.5422.1954

Duan, F. and Wang, J., Fluid–Structure–Sound Interaction in Noise Reduction of a Circular Cylinder with Flexible Splitter Plate, *J. Fluid Mech.*, vol. **920**, 2021.

Ellington, C.P., The Novel Aerodynamics of Insect Flight: Applications to Micro-Air Vehicles, *J. Exp. Biol.*, vol. **202**, no. 23, pp. 3439–3448, 1999.

Gluck, M., Breuer, M., Durst, F., Halfmann, A., and Rank, E., Computation of Fluid-Structure Interaction on Lightweight Structures, *J. Wind Eng. Ind. Aerodyn.*, vol. **89**, nos. 14–15, pp. 1351–1368, 2001. DOI: 10.1016/S0167-6105(01)00150-7

Goushcha, O., Elvin, N., and Andreopoulos, Y., Interactions of Vortices with a Flexible Beam with Applications in Fluidic Energy Harvesting, *Appl. Phy. Lett.*, vol. **104**, no. 2, pp. 2012–2017, 2014. DOI: 10.1063/1.4861927

Heathcote, S., Martin, D., and Gursul, I., Flexible Flapping Airfoil Propulsion at Zero Freestream Velocity, *AIAA J.*, vol. **42**, no. 11, pp. 2196–2204, 2004. DOI: 10.2514/1.5299

Heathcote, S., Wang, Z., and Gursul, I., Effect of Spanwise Flexibility on Flapping Wing Propulsion, *J. Fluids Struct.*, vol. **24**, no. 2, pp. 183–199, 2008. DOI: 10.1016/j.jfluidstructs.2007.08.003

Ho, S., Nassef, H., Pornsinsirirak, N., Tai, Y.-C., and Ho, C.-M., Unsteady Aerodynamics and Flow Control for Flapping Wing Flyers, *Prog. Aerosp. Sci.*, vol. **39**, no. 8, pp. 635–681, 2003. DOI: 10.1016/j.paerosci.2003.04.001

Hu, H., Kumar, A., Abate, G., and Albertani, R., An Experimental Study of Flexible Membrane Wings in Flapping Flight, *Proc. of 47th AIAA Aerospace Sciences*, pp. 1–16, 2009. doi: 10.2514/6.2009-876

Hu, Y. and Wang, J.J., The Effects of Attached Flexible Tail Length on the Flow Structure of an Oscillating Cylinder, *Sci. China Phys. Mech. Astron.*, vol. **56**, no. 2, pp. 340–352, 2013. DOI: 10.1007/s11433-013-5014-8

Hu, Y., Pan, C., and Wang, J. J., Vortex Structure for Flow over a Heaving Cylinder with a Flexible Tail, *Exp. Fluids*, vol. **55**, no. 2, 2014. DOI: 10.1007/s00348-014-1682-z

Hua, R.-N., Zhu, L., and Lu, X.-Y., Locomotion of a Flapping Flexible Plate, *Phys. Fluids*, vol. **25**, no. 12, p. 121901, 2013. DOI: 10.1063/1.4832857

Jin, Y., Kim, J.-T., Hong, L., and Chamorro, L.P., Flow-Induced Oscillations of Low-Aspect-Ratio Flexible Plates with Various Tip Geometries, *Phys. Fluids*, vol. **30**, no. 9, p. 097102, 2018. DOI: 10.1063/1.5046950

Jukes, T.N. and Choi, K.-S., Flow Control around a Circular Cylinder Using Pulsed Dielectric Barrier Discharge Surface Plasma, *Phys. Fluids*, vol. **21**, no. 8, p. 084103, 2009. DOI: 10.1063/1.3194307

Kang, C.-K., Aono, H., Cesnik, C.E.S., and Shyy, W., Effects of Flexibility on the Aerodynamic Performance of Flapping Wings, *J. Fluid Mech.*, vol. **689**, pp. 32–74, 2011. DOI: 10.1017/jfm.2011.428

Kundu, A., Soti, A.K., Bhardwaj, R., and Thompson, M.C., The Response of an Elastic Splitter Plate Attached to a Cylinder to Laminar Pulsatile Flow, *J. Fluids Struct.*, vol. **68**, pp. 423–443, 2017. DOI: 10.1016/j.jfluidstructs.2016.11.011

Lee, J.H., Huang, W.-X., and Sung, H.J., Flapping Dynamics of a Flexible Flag in a Uniform Flow, *Fluid Dyn. Res.*, vol. **46**, no. 5, p. 055517, 2014. DOI: 10.1088/0169-5983/46/5/055517

Lee, J. and You, D., Study of Vortex-Shedding-Induced Vibration of a Flexible Splitter Plate behind a Cylinder, *Phys. Fluids*, vol. **25**, no. 11, p. 110811, 2013. DOI: 10.1063/1.4819346

Liang, S., Wang, J., Xu, B., Wu, W., and Lin, K., Vortex-Induced Vibration and Structure Instability for a Circular Cylinder with Flexible Splitter Plates, *J. Wind Eng. Ind. Aerodyn.*, vol. **174**, pp. 200–209, 2018. DOI: 10.1016/j.jweia.2017.12.030

Marais, C., Thiria, B., Wesfreid, J.E., and Godoy-Diana, R., Stabilizing Effect of Flexibility in the Wake of a Flapping Foil, *J. Fluid Mech*., vol. **710**, pp. 659–669, 2012. DOI: 10.1017/jfm.2012.390

Mat Ali, M.S., Doolan, C.J., and Wheatley, V., Low Reynolds Number Flow over a Square Cylinder with a Splitter Plate, *Phys. Fluids*, vol. **23**, no. 3, p. 033602, 2011. DOI: 10.1063/1.3563619

Mazaheri, K. and Ebrahimi, A., Experimental Study on Interaction of Aerodynamics with Flexible Wings of Flapping Vehicles in Hovering and Cruise Flight, *Arch. Appl. Mech.*, vol. **80**, no. 11, pp. 1255–1269, 2010. DOI: 10.1007/s00419-009-0360-8

Miao, J.-M. and Ho, M.-H., Effect of Flexure on Aerodynamic Propulsive Efficiency of Flapping Flexible Airfoil, *J. Fluids Struct.*, vol. **22**, no. 3, pp. 401–419, 2006. DOI: 10.1016/j.jfluidstructs.2005.11.004

Noel, J., Yadav, R., Li, G., and Daqaq, M.F., Improving the Performance of Galloping Micro-Power Generators by Passively Manipulating the Trailing Edge, *Appl. Phys. Lett.*, vol. **112**, no. 8, pp. 1–6, 2018. DOI: 10.1063/1.5016102

Owen, J.C., Szewczyk, A.A., and Bearman, P.W., Suppression of Kármán Vortex Shedding, *Phys. Fluids*, vol. **12**, no. 9, p. S9, 2000. DOI: 10.1063/1.4739170

Park, H., Lee, D., Jeon, W.-P., Hahn, S., Kim, J., Kim, J., Choi, J., and Choi, H., Drag Reduction in Flow over a Two-Dimensional Bluff Body with a Blunt Trailing Edge Using a New Passive Device, *J. Fluid Mech.*, vol. **563**, p. 389, 2006. DOI: 10.1017/S0022112006001364

Qin, J., Li, L., Hao, Y., Xu, J., Bai, F., and Ye, J., Analysis of Aerodynamic Characteristics of Flexible Flapping Flap with Bidirectional Fluid-Structure Interaction, *AIP Adv.*, vol. **10**, no. 10, p. 105108, 2020. DOI: 10.1063/5.0021567

Rastan, M.R., Sohankar, A., Doolan, C., Moreau, D., Shirani, E., and Alam, M.M., Controlled Flow over a Finite Square Cylinder Using Suction and Blowing, *Int. J. Mech. Sci.*, vol. **156**, pp. 410–434, 2019. DOI: 10.1016/j.ijmecsci.2019.04.013

Razavi, S.E., Osanloo, B., and Sajedi, R., Application of Splitter Plate on the Modification of Hydro-Thermal Behavior of PPFHS, *Appl. Therm. Eng.*, vol. **80**, pp. 97–108, 2015. DOI: 10.1016/j.applthermaleng.2015.01.046

Roshko, A., *On the Development of Turbulent Wakes from Vortex Streets*, National Advisory Committee for Aeronautics, Washington, DC, from https://resolver.caltech.edu/CaltechAUTHORS:ROSnacarpt1191, 1954.

Ryu, J., Park, S.G., Huang, W.X., and Sung, H.J., Hydrodynamics of a Three-Dimensional Self-Propelled Flexible Plate, *Phys. Fluids*, vol. **31**, no. 2, p. 021902, 2019. DOI: 10.1063/1.5064482

Ryu, J., Park, S.G., Kim, B., and Sung, H.J., Flapping Dynamics of an Inverted Flag in a Uniform Flow, *J. Fluids Struct.*, vol. **57**, pp. 159–169, 2015. DOI: 10.1016/j.jfluidstructs.2015.06.006

Sahu, T.R., Furquan, M., Jaiswal, Y., and Mittal, S., Flow-Induced Vibration of a Circular Cylinder with Rigid Splitter Plate, *J. Fluids Struct.*, vol. **89**, pp. 244–256, 2019. DOI: 10.1016/j.jfluidstructs.2019.03.015

Sajedi, R., Osanloo, B., Talati, F., and Taghilou, M., Splitter Plate Application on the Circular and Square Pin Fin Heat Sinks, *Microelectron. Reliab.*, vol. **62**, pp. 91–101, 2016. DOI: 10.1016/j.microrel.2016.03.026

Sane, S.P. and Dickinson, M.H., The Aerodynamic Effects of Wing Rotation and a Revised Quasi-Steady Model of Flapping Flight, *J. Exp. Biol.*, vol. **205**, no. 8, pp. 1087–1096, 2002.

Satheesh, S., Díaz-Ojeda, H.R., González, L.M., and Huera-Huarte, F.J., Hydrodynamic Forces on a Cylinder with a Flexible Splitter Plate Near the Free Surface, *J. Offshore Mech. Arct. Eng.*, vol. **142**, no. 6, p. 061202, 2020. DOI: 10.1115/1.4047199

Sharma, K.R. and Dutta, S., IHMTC2017-01-1370, *IHMTC-2017, Proc. of 24th National and 2nd Int. ISHMT-ASTFE Heat and Mass Transfer Conf.*, ISHMTC Digital Library, pp. 1087–1094, 2017.

Sharma, K.R. and Dutta, S., Flow over a Square Cylinder with an Attached Cambered Flexible Wake Splitter, *Proc. of Topical Problems of Fluid Mechanics 2019*, D. Šimurda and T. Bodnár, Eds., pp. 109–116, 2019.

Sharma, K.R. and Dutta, S., Flow Control over a Square Cylinder Using Attached Rigid and Flexible Splitter Plate at Intermediate Flow Regime, *Phys. Fluids*, vol. **32**, no. 1, p. 014104, 2020a. DOI: 10.1063/1.5127905

Sharma, K.R. and Dutta, S., Wake Sensitivity of Flow over a Square Cylinder with Respect to Length of an Attached Flexible Wake Splitter, *J. Flow Visualiz. Image Process.*, vol. **27**, no. 3, pp. 269–296, 2020b.

Sharma, K.R. and Dutta, S., Influence of Length and Effective Stiffness of an Attached Flexible Foil for Flow over a Square Cylinder, *J. Fluids Struct.*, vol. **104**, p. 103298, 2021. DOI: 10.1016/j.jfluidstructs.2021.103298

Shen, P., Lin, L., Wei, Y., Dou, H., and Tu, C., Vortex Shedding Characteristics around a Circular Cylinder with Flexible Film, *Eur. J. Mech. B Fluids*, vol. **77**, pp. 201–210, 2019. DOI: 10.1016/j.euromechflu.2019.05.008

Shinde, S.Y. and Arakeri, J.H., Flexibility in Flapping Foil Suppresses Meandering of Induced Jet in Absence of Free Stream, *J. Fluid Mech.*, vol. **757**, pp. 231–250, 2014. DOI: 10.1017/jfm.2014.480

Shukla, S., Govardhan, R.N., and Arakeri, J.H., Flow over a Cylinder with a Hinged-Splitter Plate, *J. Fluids Struct.*, vol. **25**, no. 4, pp. 713–720, 2009. DOI: 10.1016/j.jfluidstructs.2008.11.004

Shukla, S., Govardhan, R.N., and Arakeri, J.H., Dynamics of a Flexible Splitter Plate in the Wake of a Circular Cylinder, *J. Fluids Struct.*, vol. **41**, pp. 127–134, 2013. DOI: 10.1016/j.jfluidstructs.2013.03.002

Song, J., Hu, G., Tse, K.T., Li, S.W., and Kwok, K.C.S., Performance of a Circular Cylinder Piezoelectric Wind Energy Harvester Fitted with a Splitter Plate, *Appl. Phys. Lett.*, vol. **111**, no. 22, pp. 1–5, 2017. DOI: 10.1063/1.5008918

Sosa, R., Artana, G., Benard, N., and Moreau, E., Mean Lift Generation on Cylinders Induced with Plasma Actuators, *Exp. Fluids*, vol. **51**, no. 3, pp. 853–860, 2011. DOI: 10.1007/s00348-011-1108-0

Sun, M. and Tang, J., Unsteady Aerodynamic Force Generation by a Model Fruit Fly Wing in Flapping Motion., *J. Exp. Biol.*, vol. **205**, no. 1, pp. 55–70, 2002.

Sun, X., Suh, C.S., Sun, C., and Yu, B., Vortex-Induced Vibration of a Flexible Splitter Plate Attached to a Square Cylinder in Laminar Flow, *J. Fluids Struct.*, vol. **101**, p. 103206, 2021. DOI: 10.1016/j.jfluidstructs.2020.103206

Teksin, S. and Yayla, S., Effects of Flexible Splitter Plate in the Wake of a Cylindrical Body, *J. Appl. Fluid Mech*., vol. **9**, no. 6, pp. 3053–59, 2016.

Teksin, S. and Yayla, S., Effects of Flexible Plate Attached to the Rear of the Cylinder on Flow Structure, *J. Mech. Sci. Technol.*, vol. **31**, no. 3, pp. 1195–1201, 2017. DOI: 10.1007/s12206-017-0218-y

Thomas, F.O., Kozlov, A., and Corke, T.C., Plasma Actuators for Cylinder Flow Control and Noise Reduction, *AIAA J.*, vol. **46**, no. 8, pp. 1921–1931, 2008. DOI: 10.2514/1.27821

Tronchin, T., David, L., and Farcy, A., Loads and Pressure Evaluation of the Flow around a Flapping Wing, *PIV13*, *Proc. of 10th Int. Symp. on Particle Image Velocimetry*, 2013.

von Ellenrieder, K.D., Parker, K., and Soria, J., Fluid Mechanics of Flapping Wings, *Exp. Therm. Fluid Sci.*, vol. **32**, no. 8, pp. 1578–1589, 2008. DOI: 10.1016/j.expthermflusci.2008.05.003

Warui, H.M. and Fujisawa, N., Feedback Control of Vortex Shedding by Cross-Flow Cylinder Oscillations, *Exp. Fluids*, vol. **21**, pp. 49–56, 1996.

Watman, D. and Furukawa, T., A Visualization System for Analysis of Micro Aerial Vehicle Scaled Flapping Wings, *J. Intell. Rob. Syst.*, vol. **51**, no. 3, pp. 369–381, 2008. DOI: 10.1007/s10846-007-9191-4

Wu, J., Qiu, Y.L., Shu, C., and Zhao, N., Flow Control of a Circular Cylinder by Using an Attached Flexible Filament, *Phys. Fluids*, vol. **26**, no. 10, p. 103601, 2014a. DOI: 10.1063/1.4896942

Wu, J., Shu, C., and Zhao, N., Investigation of Flow Characteristics around a Stationary Circular Cylinder with an Undulatory Plate, *Eur. J. Mech. B Fluids*, vol. **48**, pp. 27–39, 2014b. DOI: 10.1016/j.euromechflu.2014.04.007

Wu, J., Shu, C., and Zhao, N., Numerical Investigation of Vortex-Induced Vibration of a Circular Cylinder with a Hinged Flat Plate, *Phys. Fluids*, vol. **26**, no. 6, p. 063601, 2014c. DOI: 10.1063/1.4880135

Wu, J. and Shu, C., Numerical Study of Flow Characteristics behind a Stationary Circular Cylinder with a Flapping Plate, *Phys. Fluids*, vol. **23**, no. 7, p. 073601, 2011. DOI: 10.1063/1.3601484

Xiao, Q., Liu, W., and Hu, J., Parametric Study on a Cylinder Drag Reduction Using Downstream Undulating Foil, *Eur. J. Mech. B Fluids*, vol. **36**, pp. 48–62, 2012. DOI: 10.1016/j.euromechflu.2012.04.005

Xiao, Q., Sun, K., Liu, H., and Hu, J., Computational Study on near Wake Interaction between Undulation Body and a D-Section Cylinder, *Ocean Eng.*, vol. **38**, no. 4, pp. 673–683, 2011. DOI: 10.1016/j.oceaneng.2010.12.017

Yayla, S. and Teksin, S., Flow Measurement around a Cylindrical Body by Attaching Flexible Plate: A PIV Approach, *Flow Meas. Instrum.*, vol. **62**, pp. 56–65, 2018. DOI: 10.1016/j.flowmeasinst.2018.05.003

Yayla, S., Teksin, S., and Sahin, B., Control of Flow Structures around a Cylinder in Deep Water Employing a Passive Control Element, *Fluid Dyn. Res.*, vol. **51**, no. 5, p. 055512, 2019. DOI: 10.1088/1873-7005/ab3e1b

Yu, X. and Yu, X., Laboratory Evaluation of Time-Domain Reflectometry for Bridge Scour Measurement: Comparison with the Ultrasonic Method, *Adv. Civ. Eng.*, vol. **2010**, p. 508172, 2010. DOI: 10.1155/2010/508172

Zhang, Y. and Zhu, K., Flow over an Inline Oscillating Circular Cylinder in the Wake of a Stationary Circular Cylinder, *Fluid Dyn. Res.*, vol. **49**, no. 1, p. 015504, 2017. DOI: 10.1088/0169-5983/49/1/015504

Zhou, X., Wang, J.J., and Hu, Y., Experimental Investigation on the Flow around a Circular Cylinder with Upstream Splitter Plate, *J. Visualiz.*, vol. **22**, 683–695, 2019. DOI: 10.1007/s12650-019-00560-x